fluids

MDPI

Review

Aircraft Icing: Droplet Impact, Post-Impact Motion, Ice Accretion, and Mitigation Strategies

Matthew Tamarin, Taveed Tamarin and Sara Moghtadernejad *

Department of Chemical Engineering, California State University Long Beach, Long Beach, CA 90840, USA
* Correspondence: sara.moghtadernejad@csulb.edu; Tel.: +1-562-985-7534

Abstract

Aircraft icing couples droplet transport, impact, surface-water motion, nucleation, and freezing. This narrative review examines how these processes produce aircraft hazards and constrain ice-protection choices. Targeted literature searches support comparisons of laboratory conditions, measurement methods, validation evidence, and limits of transfer to flight. Particular attention is given to pre-impact deformation and breakup, local impact conditions, and the transport of unfrozen water as films, rivulets, and droplets over an airfoil. We link wettability to contact-line retention and heterogeneous nucleation while distinguishing the water contact angle from the ice-nucleus contact angle in classical nucleation theory. The review relates these mechanisms to structural, ground, induction-system, instrument, and ice-crystal icing. Established thermal, pneumatic, and fluid-based systems are distinguished from developing ultrasonic and passive-surface approaches. Sensing and machine learning are treated as facilitating technologies for diagnosis and control, rather than independent ice-removal mechanisms. The synthesis identifies local water retention, freezing fraction, runback, and removal performance as complementary evaluation outcomes. Remaining needs include measurements under representative impact and airflow conditions, uncertainty reporting, coating durability, and validation of integrated protection systems.

Keywords: aircraft icing; droplet impact; droplet dynamics; supercooled water droplets; droplet solidification; ice nucleation; ice accretion; wettability; heat transfer; ice-protection systems

1. Introduction

Aircraft icing is a multidisciplinary safety problem governed by interactions among meteorology, fluid mechanics, heat transfer, surface science, and aircraft operations. Supercooled water droplets and, in some environments, ice crystals interact with aircraft surfaces and systems, producing accretion that can modify aerodynamic geometry, obstruct sensors and engine passages, and reduce the reliability of flight information. A droplet-centered description is therefore useful because the transition from atmospheric moisture to hazardous ice begins with transport, impact, interfacial motion, heat exchange, and phase change at the surface [1–3].

Icing affects wind turbines, heat exchangers, agriculture, and aviation. Droplet impacts, shedding, and coalescence on surfaces underlie ice formation in these settings [4]. Freezing affects crops such as wheat [5]. Dedicated icing facilities, such as the Braunschweig Icing Wind Tunnel, are used to study ice accretion on structures [6]. Frosting degrades heat-exchanger performance [7], and ice alters the structural behavior of wind turbines [8].

Check for updates

Academic Editor: Xuemin Ye

Received: 7 October 2026
Revised: 10 November 2026
Accepted: 11 November 2026
Published: 12 November 2026

Copyright: © 2026 by the authors. Licensee MDPI, Basel, Switzerland. This article is an open access article distributed under the terms and conditions of the Creative Commons Attribution (CC BY) license.

Although these effects occur across many sectors, this review focuses on aviation because aircraft icing simultaneously challenges aerodynamic performance, propulsion, sensing, and operational safety [1].

Weather has constrained aviation since the earliest powered flights [9]. Aircraft icing became a prominent operational problem during the expansion of U.S. Air Mail routes in the 1920s [10]. Protection includes anti-icing, which prevents or delays ice accretion, and de-icing, which removes ice after it has formed. These terms refer to physical protection functions; sensing, forecasting, and data-assisted control can support their operation.

Subsequent research combined natural-icing flight tests with controlled laboratory facilities that reproduced icing conditions more safely and repeatably. Early studies included icing-tunnel development in the 1940s and the 1948 C-46 natural-icing tests performed by Preston and Blackman [2,9]. Modern facilities include the National Aeronautics and Space Administration (NASA) Glenn Icing Research Tunnel and the Italian Aerospace Research Centre (CIRA) Icing Wind Tunnel in Italy [1].

Despite decades of study, important gaps remain because icing behavior depends on coupled meteorological conditions, droplet-size distributions, aircraft geometry, surface state, and protection-system limits. These gaps motivate continued work on droplet and ice physics, device performance under representative conditions, and durable icephobic and hybrid protection concepts [2,3,6,11,12].

Accordingly, this review adopts a mechanism-to-application approach. It treats droplet transport and impact as the starting point for understanding freezing, runback, ice morphology, aircraft-level consequences, and protection-system selection. This structure supports comparison of mitigation concepts according to the droplet or ice process that each method modifies. In keeping with this perspective, the formation and movement of droplets (how they are transported to a surface; how they spread, recede, rebound, slide, or are sheared downstream; and where they ultimately freeze) are placed at the center of the analysis.

Guo et al. [13] provide a detailed review, centered on supercooled large droplets (SLDs), of normal impacts on dry and wet surfaces, complex impact scenarios, coupled surface-water transport and freezing, and emerging ice-protection surfaces. These subjects overlap with Section 2 of the present review; a new account of SLD impact physics is therefore not claimed. The specific differences are in scope, analytical emphasis, and the resulting assessment. First, the present review connects droplet physics to structural, ground, propulsion, instrument, and ice-crystal icing. Second, it examines heterogeneous nucleation, laboratory-to-flight transfer, and the distinction between local impact and upstream droplet conditions. Third, its protection comparison separates operational systems, emerging concepts, and facilitating diagnostic technologies, leading to evidence requirements for selecting and validating a protection method. The detailed SLD splash correlations covered in [13] are summarized only as context. Additional primary studies on frozen-splat peeling, spreading arrest, rebound/adhesion, and grooved surfaces extend the comparison of impact and freezing outcomes [14–17].

Review Approach

This narrative review was supplemented by targeted electronic searches (conducted on 26 October 2026) of publisher records, author manuscripts, the NASA Technical Reports Server (NTRS), and official aviation sources, without a lower publication-year limit. Sources were selected for relevance to aircraft icing, droplet impact/freezing, surface-water transport, protection, and associated hazards. Primary experiments and simulations informed mechanistic comparisons, reviews provided context, and official reports supplied operational and accident information. Evidence quality was assessed qualitatively from reported

conditions, methods, uncertainty, and validation information (Section 2.1.8); exhaustive retrieval is not claimed.

2. Droplet-Scale Physics of Aircraft Icing

This section reviews the principal parameters governing droplet impact, solidification, and nucleation. Foundational observations of droplet impact trace to Worthington [18,19], and subsequent work has resolved increasingly complex thermal and interfacial regimes. These coupled processes determine liquid retention, runback, and the initial development of aircraft ice accretion.

Aircraft ice accretion begins with interactions among supercooled droplets, airflow, and cold surfaces. Droplet-impact physics is considered here when it helps explain whether water spreads, rebounds, splashes, runs back, or freezes on an aircraft component. At the environmental scale, icing may be described as precipitation icing, in-cloud icing, or hoarfrost icing [20–22]. Precipitation icing accompanies freezing precipitation or frozen hydrometeors; in-cloud icing occurs when supercooled liquid droplets impinge on exposed surfaces; and hoarfrost forms by vapor deposition on sufficiently cold surfaces. Aircraft structural icing is primarily associated with in-cloud or precipitation encounters involving supercooled liquid water [1,2,9,10,22–24]. Rime, glaze (clear), and mixed ice describe accretion morphologies and are discussed in Section 3.3.

2.1. Parameters Governing Droplet Impact and Solidification

Droplet solidification is closely coupled with impact on solid surfaces. Experiments identify six principal outcomes for impact on dry surfaces: deposition, receding breakup, partial rebound, complete rebound, prompt splash, and corona splash [25–32]. The observed regime depends on droplet properties, impact conditions, and surface characteristics. Post-impact motion includes spreading to a maximum diameter, capillary-driven receding, partial or complete rebound, and breakup into secondary droplets [31,33–36].

The outcome is governed by coupled droplet, surface, and flow conditions rather than by one parameter alone. This review therefore considers airflow and impact velocity, liquid and surface temperature, droplet size and shape, surface wettability, surface chemistry and contamination, relative surface motion, and surface orientation [31,33,37–39]. These factors are emphasized because they connect droplet-impact dynamics to freezing, runback, and ice-protection performance. Each subsection first summarizes the relevant mechanism and then identifies how it has been used, or could be used, to reduce icing.

A low-speed isolated-drop experiment is useful for identifying a mechanism, but its aircraft relevance depends on the local impact state and thermal boundary conditions. Before contact, small droplets can follow deflected streamlines while higher inertia drops depart from them; geometry and droplet drag set the impingement limits [40]. Vargas et al. documented pre-impact deformation and breakup for 500–1800 μm droplets interacting with airfoils at 70 and 90 m/s [41]. These aerodynamic observations support using the arriving size/velocity distribution, not treating a quiescent falling millimeter drop as a complete flight surrogate.

2.1.1. Airflow and Impact Velocity

Airflow affects impact velocity and the subsequent transport of liquid water across a surface [33]. Higher impact velocity increases droplet inertia and generally facilitates a larger maximum spreading diameter as normal momentum is redirected along the surface [31,42]. The resulting contact area can enhance heat transfer to a sufficiently cold substrate and influence freezing time [28,31,34,42,43]. At sufficiently high inertia, however, splashing and secondary-droplet formation may reduce the liquid mass retained at the initial impact

site. Recent supercooled-large-droplet studies reinforce that relative velocity, droplet size, and surface temperature should be evaluated together when translating laboratory impact regimes to aircraft conditions [13,37,44].

Comparability requires more than equal impact Weber numbers. A high-airflow test may introduce pre-impact deformation, obliquity, gas entrainment, and repeated wet impacts that are absent from a dry-plate test. The historical splash threshold below is therefore a condition-specific correlation, not a universal aircraft criterion. Gas density and slip velocity govern aerodynamic deformation, while liquid inertia and local surface-relative velocity govern the conventional impact number. The spreading-arrest experiments compared in Section 2.1.8 used droplet impact speeds of 0.10–1.10 m/s [15]. The cold-flow experiments used 2.6 mm droplets impacting at 1.6 m/s while the imposed airflow varied from 0 to 10 m/s [45]. These droplet impact speeds must be distinguished from the airfoil speeds of 70 and 90 m/s in the breakup experiments [41] and the 87 m/s tunnel airspeed in the accretion tests discussed in Section 2.1.8. The comparison illustrates a gap in test conditions; transfer to flight requires the local droplet velocity relative to the surface, not the aircraft or tunnel airspeed alone.

A common dimensionless measure of droplet-impact inertia relative to surface tension is the Weber number, given in Equation (1) [31,33].

$$We = \frac{\rho U^2 D}{\sigma} \tag{1}$$

In Equation (1), ρ is liquid density, σ is liquid surface tension, D is the equivalent-volume diameter of the droplet reaching the surface, and U is its velocity relative to the local surface immediately before contact. For a normal impact, U is the normal impact speed. For an oblique impact, the normal and tangential components must be reported separately, and the convention used in a correlation must be retained. If an upstream SLD breaks up, the parent diameter cannot simply be substituted for the sizes of the fragments that arrive at the surface [40,41]. Aerodynamic breakup instead uses a gas-based Weber number, $We_g = \rho_g |u_g - u_d|^2 D/\sigma$, where ρ_g is gas density and $u_g - u_d$ is the local gas–droplet slip velocity; it must not be confused with the liquid-based impact Weber number.

Viscous effects are commonly characterized by the Reynolds number, $Re = \rho U D/\mu$, and the Ohnesorge number, $Oh = \mu/\sqrt{(\rho\sigma D)} = \sqrt{We}/Re$, where μ is the liquid dynamic viscosity [29,31]. For impacts on dry, smooth surfaces, the onset of splashing is often expressed through the combined parameter K_s defined in Equation (2) [29,46].

$$K_s = We^{1/2} Re^{1/4} \tag{2}$$

Mundo et al. observed splashing above $K_s \approx 57.7$ in their dry, smooth-surface experiments [46]. The threshold, however, decreases with surface roughness and depends on ambient gas pressure, wettability, and pre-existing liquid films, so such criteria should be transferred to aircraft surfaces with caution [29,32]. The high relative velocity of supercooled large droplets can place their impacts well inside the splashing regime, which is why splashing and the re-entrainment of secondary droplets must be considered when estimating SLD collection efficiency [13].

Illustrative scaling estimates clarify the gap between laboratory and flight conditions. Using approximate water properties near 0 °C (density 1000 kg/m^3, surface tension 0.0756 N/m, dynamic viscosity 1.79 mPa·s, and thermal diffusivity $\alpha_l = 1.33 \times 10^{-7}$ m^2/s), the spreading-arrest experiment [15] at $D = 2.0$ mm and $U = 1.10$ m/s gives $We \approx 32$ and $K_s \approx 33$; the cold-flow experiment [45] at $D = 2.6$ mm and $U = 1.6$ m/s gives $We \approx 88$ and $K_s \approx 65$. These are illustrative property-based estimates, not the original studies' reported dimensionless values. Using 70 m/s as an assumed velocity scale gives $We \approx 1300$ and $K_s \approx 190$ for a 20 µm droplet, and $We \approx 13{,}000$ and $K_s \approx 1100$ for a 200 µm droplet. These

flight-scale estimates use an assumed intact droplet and free-stream velocity; they are not measured local impact conditions or rigorous bounds. Pre-impact deformation, breakup, trajectory deflection, and impact obliquity must be resolved before applying a local impact correlation [40,41]. Nor does comparison with the dry-surface threshold $K_s \approx 57.7$ [46] establish a splashing outcome on a cold, wet, or textured surface. The thermal Péclet number $Pe = UD/\alpha_l$ is approximately 2×10^4–3×10^4 for these laboratory examples and 10^4–10^5 for the assumed flight-scale examples. Thus, the time D/U is shorter than the full-droplet diffusion time D^2/α_l in each example. This comparison does not establish the ordering of recoil, nucleation, contact-line freezing, or complete solidification, which also depends on supercooling, latent heat, substrate thermal properties, and interfacial heat transfer. Laboratory findings can identify mechanisms, but matching Pe alone does not establish thermal similarity to flight.

Airflow also drives liquid that remains unfrozen after impact. An isolated drop can elongate or be swept from the surface. Under repeated impingement, neighboring drops may coalesce and sustain a film; breakup of this film can then produce rivulets [13,47,48]. These configurations have different contact-line and heat-transfer behavior. Their practical consequences on an airfoil are developed in Section 2.1.8, rather than inferred from drop spreading alone.

2.1.2. Liquid and Surface Temperature

Liquid and surface temperature affect both post-impact droplet motion and freezing. On a sufficiently cold surface, a supercooled droplet can nucleate and solidify through precooling, nucleation, rapid recalescence, heat-transfer-controlled freezing, and post-freezing cooling. During recalescence, crystal growth and latent-heat release raise the droplet toward its equilibrium freezing temperature; subsequent solidification proceeds as heat is removed through the surface and surrounding flow [35,49,50]. Surface temperature also affects recoil. Li et al. reported that supercooling had little effect on initial spreading but reduced receding speed and height when the receding period was sufficiently long [51].

Droplet and surface temperatures must be distinguished. Increased liquid viscosity can reduce recoil, while rapid interfacial freezing can arrest motion independently of that viscosity change [15,16,38,52,53]. An experiment with room-temperature water on a cold plate is therefore not thermally equivalent to impact of supercooled cloud water, even when the substrate temperature and Weber number match. The substrate thermal properties and the interfacial temperature also affect how quickly spreading is arrested.

Heated surfaces can inhibit freezing. Depending on temperature and heat flux, an impacting droplet may undergo evaporation, nucleate boiling, transition boiling, or film boiling [33,43]. At or above the Leidenfrost temperature, a continuously replenished vapor layer can separate the droplet from the surface [33,54–56]. For aircraft protection, the directly relevant case is intentional heating above the local freezing threshold, which underlies the thermal anti-icing and de-icing methods discussed in Section 4.1.

Surface temperature also affects how long liquid remains mobile before it freezes or is displaced. Frost and evolving surface roughness can increase pinning and shorten shear-driven rivulets, whereas sufficiently strong aerodynamic shear can overcome this retention and transport water downstream [4,47]. The net icing consequence depends on competing effects on retention, wetted area, and freezing rate.

These studies illustrate why a single temperature trend is inadequate. Gorin et al. linked reduced spreading to the growth of a frozen layer that arrests the contact line [15]. Zhang et al. coupled supercooling and dynamic contact angle in experiments and simulations, reporting a maximum 11.3% discrepancy in spreading factors between model and experiment; this is a validation discrepancy, not a measurement uncertainty [16]. Fang et al.

found that sufficiently cold hydrophobic copper can instead promote later thermomechanical peeling of the frozen splat [14]. Earlier arrest and later release concern different times and cannot be ranked using freezing time alone.

2.1.3. Droplet Size and Shape

Droplet size changes inertia, thermal mass, and impact duration. Pan et al. observed longer total freezing times for larger droplets under their tested conditions [42], but this is not a size-only law for a wing. The freezing time of an isolated millimeter drop cannot be equated to the freezing fraction of a continuously replenished cloud-droplet film. Pre-impact breakup further replaces a parent SLD with a distribution of smaller fragments, changing both retained water and the relevant local impact parameters [13,41,44].

Surface topography can alter droplet shape and the direction and extent of spreading and retraction [33]. Grooves and anisotropic patterns create direction-dependent energy barriers that elongate the wetted footprint, while asymmetric nanostructures can promote preferential spreading in one direction [57–62]. These changes redistribute liquid–solid contact and therefore the locations of heat transfer and freezing. Their relevance to engineered superhydrophobic and patterned surfaces is discussed further in Section 4.4.

Hosseini et al. varied groove dimensions, Weber number, and supercooling in an axisymmetric numerical study [17]. Its trapped-air geometry and imposed freezing treatment differ from open, three-dimensional texture on an aircraft. The resulting rebound limits should therefore be treated as model- and geometry-specific. A numerical change in outcome can reflect the contact-angle or phase-change closure as well as a physical surface effect.

2.1.4. Surface Wettability

Surface wettability describes how readily a liquid spreads over and remains in contact with a solid, making it directly relevant to ice accretion. A common descriptor is the static contact angle, θ, measured through the liquid at the solid–liquid–gas contact line [33]. In the experiments conducted by Pan et al., an increasing contact angle was associated with longer total freezing time [42], although contact-angle hysteresis, roughness, impact conditions, and nucleation sites also influence icing behavior.

A useful first distinction is between hydrophilic and hydrophobic surfaces, as illustrated in Figure 1. Hydrophobic surfaces reduce equilibrium wetting and may delay freezing or reduce ice-removal energy under some conditions [47,63,64]. Hydrophilic surfaces promote spreading and can form longer wetted regions or rivulets, increasing the area over which freezing may occur [47,57,65–70]. Wettability alone, however, does not determine icephobic performance. The link between wetting and heterogeneous nucleation is developed in Section 2.2.2, where the ice-embryo contact angle is distinguished from the water contact angle used here.

Contact angle alone cannot rank aircraft anti-icing performance. A small, wetted footprint, a delayed nucleation event, and low ice adhesion are different outcomes. Gorin et al. observed spreading arrest that reduced the influence of initial wetting differences at sufficiently cold conditions [15], whereas Fang et al. observed thermally driven peeling of frozen splats on hydrophobic copper [14]. These findings concern different stages and thermal conditions; they do not establish a universal contact-angle threshold. Comparisons should report advancing/receding angles, their hysteresis, texture, thermal conditions, and whether the measured outcome is rebound, freezing onset, retained ice, or adhesion [33,42,71].

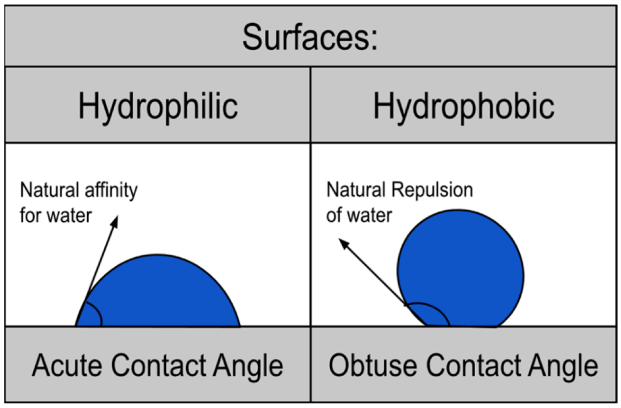

Figure 1. Surface wettability and representative hydrophilic/hydrophobic droplet shapes.

Mohammadi et al. controlled drop impact speed while varying cold airflow [45]. Their results showed improved drop repellency in one thermal regime but an extended freezing line under colder conditions. This within-study change is stronger evidence of a regime-dependent response than a comparison of unrelated surfaces tested at different temperatures. The imposed airflow nevertheless remained well below many in-flight conditions.

2.1.5. Relative Surface Motion

Relative motion between the droplet and the surface also influences droplet impact. Laboratory studies have examined droplet dynamics on both linearly translating and rotating substrates, showing that surface motion introduces a tangential velocity component that can alter spreading, deformation, and splashing behavior [33,72,73]. In experiments on a horizontally translating surface, Buksh et al. found that surface motion altered the spreading process and that liquid surface tension influenced both the time required to reach maximum spreading and the maximum spreading factor for low-viscosity liquids [73]. Moghtadernejad et al. further investigated droplet impact on a rotating aluminum disk and demonstrated that rotational speed and impact conditions produce asymmetric radial and circumferential spreading, illustrating the influence of tangential surface motion on the post-impact droplet footprint [72]. More broadly, the effects of normal and tangential impact velocities on moving-surface droplet dynamics have also been discussed in the literature [33].

For aircraft components, normal and tangential impact velocities should be evaluated in the frame of the local surface. A translating or spinning laboratory plate helps isolate tangential motion, but does not reproduce the nonuniform airflow, curvature, centrifugal loading, and repeated impingement on a propeller or rotor. Room-temperature spreading data therefore support a kinematic interpretation, not a direct prediction of frozen footprint or protection performance [33,72–74].

2.1.6. Surface Chemistry and Contamination

Surface contamination can modify wetting, nucleation, and freezing by changing the chemistry and microstructure of the liquid–solid interface [75]. Dissolved salts decrease the equilibrium freezing point, a principle used in chemical de-icing and anti-icing fluids (Section 4.3). Insoluble or deposited contaminants can instead create nucleation sites or alter contact-line pinning. Yin et al. reported lower retained contamination and greater resistance to contamination-induced changes in freezing behavior on superhydrophobic surfaces than on comparison surfaces [76]. These findings emphasize that icephobic performance must be evaluated on aged and contaminated surfaces, not only on pristine specimens.

Soluble contamination can change equilibrium phase behavior, whereas particulate deposits can alter nucleation and pinning. These effects need not act in the same direction. Comparing a single observed freezing time on two surfaces cannot distinguish them without liquid composition, deposit loading, surface characterization, and repeated freezing trials [75–77]. A freezing-probability or survival curve is more informative about stochastic nucleation than one reported onset time.

2.1.7. Surface Orientation

Surface orientation influences post-impact motion, retention, and solidification. On an inclined surface, a droplet may pass through spreading, gravity-driven gliding, relaxation, and wetting stages after the very brief initial impact [78,79]. During gliding, the advancing and receding edges move at different rates, increasing downstream displacement and the wetted area until pinning or recoil occurs [78–82]. The resulting competition among gravity, inertia, capillarity, and contact-angle hysteresis determines whether liquid is retained or transported before freezing.

Inclination also affects the likelihood that a droplet departs before freezing. When the downslope component of gravity and aerodynamic forcing exceeds contact-line retention, liquid may slide or be swept from the surface; otherwise, supercooled water can remain pinned and freeze [83]. On aircraft, local surface orientation, sweep, and angle of attack therefore influence impingement, runback, and the ultimate accretion location.

In laboratory experiments, tilting a flat test specimen (a coupon) changes the components of gravity normal and tangential to its surface, whereas changing the angle of attack of an airfoil also changes the surrounding pressure field and the collection pattern. The two operations are therefore not dynamically equivalent. Inclination results should be compared at matched normal and tangential impact components and accompanied by the aerodynamic and freezing conditions [40,78–83].

2.1.8. Transport and Freezing of Surface Water on an Airfoil

Following impact near a leading edge, liquid may recoil locally, merge with neighboring drops, or feed a film. Away from the stagnation region, aerodynamic shear generally drives mobile liquid aft, with different paths on the upper and lower surfaces. Pressure gradients, capillary forces, contact-line retention, and gravity can reinforce or oppose this motion. Films may contract into rivulets or beads; roughness, contact-angle hysteresis, and existing ice can pin their edges or divert their paths [13,40,47,48,84].

Experimental airfoil data illustrate how these effects combine. In Icing Research Tunnel tests of a NACA 23012 wing section with a 160 μm median volume diameter cloud at 195 mph (87 m/s), all impinging water ran back to the trailing edge and was blown off at a total temperature of 37 °F (2.8 °C); at 34 °F (1.1 °C), less runback occurred and an ice ridge formed just aft of the active pneumatic boot [85]. Colder temperatures froze more water forward on the boot and reduced the runback available to feed the ridge, yet the ridge did not become smaller; the authors concluded that runback was not the only controlling mechanism [85]. Increasing angle of attack shifted accreted ice toward the pressure (lower) surface and reduced it on the suction (upper) surface, and unfrozen water blown from the accretion could impinge farther downstream as secondary impingement [85]. The ridge height and location varied between nominally identical runs because of random shedding of residual ice, so the shape was not quantitatively repeatable [85]. These observations directly demonstrate downstream icing beyond a pneumatic boot; the implications for heated protection require a separate heat balance. The reported temperatures are total-air temperatures, not surface or droplet temperatures. Runback models therefore require

validation against retained water and ice location, with the thermal boundary conditions stated explicitly.

A local thin-film approximation makes the driving terms explicit. For a thin, laminar film of thickness h and dynamic viscosity μ, with no slip at a locally stationary wall and a quasi-steady velocity profile, the volume flux q per unit span (m^2/s) along surface coordinate s is approximated by Equation (3). Here τ_a is the aerodynamic shear stress, p is liquid pressure including capillary pressure, ρ is liquid density, and g_t is the component of gravity along s.

$$q = \frac{\tau_a h^2}{2\mu} - \frac{h^3}{3\mu}\left(\frac{\partial p}{\partial s} - \rho g_t\right) \quad (3)$$

Equation (3) follows from the Navier–Stokes equations under the classical thin-film (lubrication) approximations. Integrating the tangential viscous momentum balance across the film, with no slip at the wall and the imposed aerodynamic shear at the liquid–air interface, gives the shear-driven and pressure/gravity-driven contributions to q. This local relation neglects inertia and does not resolve unsteady wave dynamics or three-dimensional rivulet edges; its use in an aircraft runback model requires validation for the relevant conditions. Freezing and evaporation deplete the mobile layer, while continuing deposition replenishes it. Runback length consequently depends on water supply, transport, and heat removal together; it cannot be inferred from a spreading diameter or static contact angle alone [3,13,84]. In a running-wet heated region, water may remain mobile and refreeze after leaving the protected area, making downstream transport a design constraint [40,86].

Table 1 compares representative primary studies using their stated conditions, methods, and uncertainty or validation information. It distinguishes measured uncertainty, repeatability, model–experiment discrepancy, and information not recovered from the inspected source; none is treated as interchangeable.

Table 1. Representative evidence for droplet impact, freezing, and pre-impact breakup. Conditions refer to the specified experiments or numerical cases, not a common aircraft envelope. NR-E means that a quantitative uncertainty was not extracted from the inspected source; it does not imply zero uncertainty or that the original study contains no uncertainty analysis. VOF, volume of fluid; SD, standard deviation; MVD, median volume diameter; *LWC*, liquid water content.

Study/Process	Conditions and Parameter Range	Method and Observable	Uncertainty or Validation Evidence	Aircraft Inference and Limit
Gorin et al. [15] Spreading arrest	Water D = 2.0 mm; reported glass-series impact speeds 0.10–1.10 m/s. Compared substrate temperatures: 22 and −34 °C.	High-speed/infrared imaging; glass and aluminum; spreading and arrested diameter.	Optical up to 20,000 fps; infrared up to 400 fps. NR-E for a propagated uncertainty of arrested diameter.	Shows freezing-induced arrest. Warm isolated drops and low impact speeds do not establish cloud-drop flight performance.
Zhang et al. [16] Rebound/adhesion	Numerical sweep: D = 2.12 mm; We = 10–90; static angles 90°, 120°, 150°; supercooling 5–30 K.	Experiments plus VOF and solidification model with dynamic contact angle; full/partial rebound and adhesion.	Maximum reported model–experiment spreading-factor discrepancy 11.3%; not an experimental error bar.	Shows competition between freezing and recoil. Fixed hysteresis and axisymmetric cases constrain transfer of the regime map.
Fang et al. [14] Frozen-splat peeling	Room-temperature water D = 2.2–3.4 mm on treated copper. Example substrate −43 °C; contact angles about 62° and 119°.	High-speed imaging and thermomechanical model; cracking, partial/complete peeling.	Example angles 62 ± 0.9° and 119 ± 1.2°; peeling-time error bars are SD of three tests.	Later ice release differs from pre-freezing rebound. Smooth copper and isolated splats are not a sustained aircraft-icing demonstration.

Table 1. *Cont.*

Study/Process	Conditions and Parameter Range	Method and Observable	Uncertainty or Validation Evidence	Aircraft Inference and Limit
Hosseini et al. [17] Grooved-surface response	We = 19–50; supercooled-water temperature 253.15–273.15 K; groove dimensions 0.071–0.364 mm.	Axisymmetric VOF/enthalpy-porosity model; 20 design cases; spreading and rebound.	Comparison with two experimental cases; 10 µm refined mesh. NR-E for a comprehensive output uncertainty.	Groove/air-cushion geometry and imposed nucleation/recalescence treatment limit application to 3-D aircraft textures.
Vargas et al. [41] Pre-impact breakup	Analyzed drops 500–1800 µm; reported comparisons at airfoil speeds 70 and 90 m/s.	Moving-airfoil rig; high-speed silhouettes, centroid motion, deformation, and breakup sequence.	Resolution, thresholding, curve fits, and assumed drop shape contribute uncertainty; strong scatter in breakup location.	Direct evidence of aerodynamic deformation. A flight-like speed does not reproduce all cloud and thermal conditions.
Mohammadi et al. [45] Coupled cold airflow	D = 2.6 mm; droplet impact speed 1.6 m/s; stagnation airflow 0–10 m/s; cold-environment temperature −10 to −30 °C. Impact speed matched with/without airflow.	Cold-flow impact experiments; contact time and freezing-line extent on wettability variants.	Controlled impact-speed comparison separates airflow from impact inertia. NR-E for a common output uncertainty.	Airflow reduced contact time in one regime but extended the freezing line in another. The 10 m/s flow remains below many aircraft conditions.
Addy et al. [85] Large-droplet airfoil accretion	NACA 23012; MVD 160 µm; *LWC* 0.82 g/m^3; 195 mph (87 m/s); total temperature 5–37 °F (−15 to 2.8 °C); angle of attack −2° to 3.9°.	Icing Research Tunnel tests; photographs and centerline ice tracings; lift and drag change.	Five repeat runs at the anchor condition showed run-to-run variation in ridge height and location. NR-E for a propagated uncertainty.	Shows downstream runback and secondary impingement beyond a pneumatic boot. Single wing section; *LWC* was not varied; near-freezing ridge geometry was not quantitatively repeatable.

2.2. Nucleation

The droplet-impact parameters described above determine whether water remains on an aircraft surface and how heat is transferred after impact. For initially ice-free liquid, primary freezing requires ice nucleation, which initiates the solid phase. Once ice is present, subsequent freezing can proceed by growth of existing ice without a new primary nucleation event. Nucleation occurs when molecular or atomic clusters form a stable new phase, and its probability is highly sensitive to temperature, impurities, interfaces, and local transport. Ice can form through vapor-to-solid, vapor-to-liquid-to-solid, or liquid-to-solid pathways. Because structural aircraft icing primarily involves supercooled liquid water freezing at or near a surface, the following discussion emphasizes liquid-to-solid nucleation, particularly heterogeneous nucleation [6,77,87,88].

Ice nucleation is central to aircraft icing because it controls the onset and early development of ice accretion. The broader nucleation literature spans atmospheric science, cryopreservation, food systems, and icing on aircraft, wind turbines, and power lines. A single review cannot cover all of these areas. This section therefore introduces only the nucleation concepts needed to interpret droplet freezing and aircraft-surface accretion, while emphasizing the limitations of applying idealized nucleation models to flight-relevant surfaces [89].

2.2.1. Classical Nucleation Theory

During a first-order phase transition, liquid water can remain metastable below its equilibrium melting temperature until a stable ice nucleus forms [89]. Classical nucleation theory describes the competition between the bulk free-energy benefit of forming the new phase and the interfacial-energy cost of creating a nucleus [90]. This competition produces a critical nucleus size and an associated activation barrier.

In supercooled liquid water, molecular clusters smaller than the critical nucleus are more likely to decay, whereas clusters that reach the critical size can continue to grow [77,88,91]. The critical state corresponds to the maximum in the nucleus-formation free energy, not a stable bulk phase. Once the barrier is crossed, crystal growth and latent-heat release initiate the recalescence and slower solidification stages described in Section 2.1.2.

Within classical nucleation theory, the ice-nucleation rate can be represented in Arrhenius form by Equation (4) [77,88,89].

$$J = K\exp\left(\frac{-\Delta G}{k_B T}\right) \tag{4}$$

In Equation (4), J is the nucleation rate, K is a kinetic prefactor, ΔG is the free-energy barrier for formation of the critical nucleus, k_B is the Boltzmann constant, and T is the absolute temperature.

2.2.2. Homogeneous and Heterogeneous Nucleation

Ice nucleation may be homogeneous or heterogeneous. Homogeneous nucleation occurs without a foreign solid surface or particle, whereas heterogeneous nucleation is catalyzed by an interface or nucleating particle [77,89,92]. Because aircraft icing generally involves freezing at or near a material surface, heterogeneous nucleation is usually the more directly relevant pathway.

Atmospheric heterogeneous ice nucleation is commonly discussed in terms of deposition nucleation, immersion freezing, condensation freezing, and contact freezing [91,93]. Deposition nucleation forms ice directly from vapor on an ice-nucleating particle; immersion freezing begins from a particle already immersed in a supercooled droplet; condensation freezing accompanies liquid condensation on a particle followed by freezing; and contact freezing is triggered when an ice-nucleating particle contacts a supercooled droplet. For aircraft surface accretion, these atmospheric pathways determine the hydrometeors encountered, while nucleation at the aircraft–water interface governs the onset of surface freezing.

In the spherical-cap approximation of classical nucleation theory, a flat substrate reduces the critical free-energy barrier according to Equation (5), where $\Delta G_{hom}{}^{*}$ is the homogeneous barrier and θ_i is the contact angle of the ice embryo at the substrate, measured through the ice [90,94].

$$\Delta G_{het}{}^{*} = f(\theta_i)\Delta G_{hom}{}^{*}\,;\, f(\theta_i) = \frac{(2 + cos\ \theta_i)(1 - cos\ \theta)^2}{4} \tag{5}$$

The geometric factor lies between zero and one; a substrate that better wets the ice embryo can therefore lower the barrier and increase nucleation probability. Crucially, θ_i is not the macroscopic water-in-air angle θ in Section 2.1.4. That water angle cannot be substituted directly into the ice-nucleation factor. Roughness, cavities, chemical patches, and contaminants can alter local interfacial energies or active-site populations; their effects depend on geometry and chemistry rather than a universal monotonic roughness rule [77,94]. The ideal factor therefore explains a possible barrier reduction but does not by itself predict freezing rates on an aged, textured aircraft surface. Wetting, nucleation delay, and ice adhesion must be characterized separately.

2.3. From Droplet Impingement to Ice Accretion: Heat Balance and Modeling

Aircraft-icing analysis connects droplet-scale processes through local mass and energy balances [3,21,22,95]. Equation (6) describes impinging-water mass flux per unit surface area (kg/m^2/s), where β is local collection efficiency, *LWC* is liquid water content, and V_∞ is free-stream velocity [1,3,22]. Collection depends jointly on the droplet-size distribution, local airflow, geometry, angle of attack, and, where relevant, breakup. A single monotonic rule for β should not be assumed at every location or for deformed and fragmenting droplets [40,41]. Surface-water flux and subsequent freezing must then be evaluated separately.

$$\dot{m}_{imp} = \beta \cdot LWC \cdot V_\infty \tag{6}$$

Following Messinger [95], the freezing fraction n_0 is defined in Equation (7) as the fraction of the water entering a surface control volume, including runback from upstream, that freezes within it. Equation (7) uses a quasi-steady local control-volume balance: all three mass terms must be rates for the same control volume, or fluxes normalized by the same surface area. Incoming runback is obtained from transport across the upstream boundary; it must not be added directly to a surface-area flux without this conversion. Transient depletion or refreezing of stored water requires a separate liquid-storage term.

$$n_0 = \frac{\dot{m}_{fr}}{\dot{m}_{imp} + \dot{m}_{\mathrm{rb,in}}} \tag{7}$$

When the local heat balance permits nearly all incoming water to freeze, n_0 approaches 1, and rapid freezing near the impingement region favors rime-like accretion. When $0 < n_0 < 1$, a portion of the incoming water remains liquid and can spread or run back before freezing, favoring glaze or mixed accretion [21,22,95]. Freezing fraction is thus a useful link between the droplet-scale behavior in Sections 2.1 and 2.2 and the morphologies in Section 3.3; the final ice shape also depends on where droplets impinge, surface flow, roughness, and the evolving airflow.

Engineering icing codes build on this framework. LEWICE combines a panel-method airflow solution (with an optional Navier–Stokes solver in version 3.2) with Lagrangian droplet trajectories, a Messinger-based thermodynamic model, and an empirical SLD model [96], whereas FENSAP-ICE solves Eulerian droplet equations together with a thin-film model for runback water [84]. Recent reviews describe models for liquid-film runback, SLD splashing and rebound, ice-crystal accretion, and ice shedding [3,13], and data-driven methods are being explored to predict wind-driven runback [48]. A persistent limitation is that droplet-scale phenomena such as contact-line pinning, rivulet breakup, splashing on wet or rough surfaces, and the wettability of engineered coatings are represented by empirical sub-models calibrated over limited conditions [3,13,96]. Closing this gap requires impact and runback experiments at flight-relevant velocities, droplet sizes, and surface states that are designed explicitly to validate these sub-models.

3. Aircraft Icing

With the droplet-scale mechanisms established, the discussion now examines icing severity, the principal aircraft-icing scenarios, the resulting accretion morphologies, and the hazards produced by each. The organization keeps the link between droplet behavior and aircraft-level consequences explicit.

3.1. Icing Severity

Aircraft icing severity can be described using several related classification approaches. Current Federal Aviation Administration (FAA) guidance characterizes icing intensity operationally as trace, light, moderate, or severe according to the rate and effects of ice

accumulation and the ability of the aircraft's ice-protection system to manage that accumulation [24]. Historical icing-intensity criteria associated these categories with the distance required for ½ inch (12.7 mm) of ice to accumulate on a reference probe: approximately 80 mi for trace icing, 40 mi for light icing, 20 mi for moderate icing, and 10 mi for heavy icing in the 1964 interagency scale, which used heavy in place of severe [97]. A separate thickness-based classification reported in the aircraft-icing literature categorizes ice accumulation as light at 0.1–5.0 mm, moderate at 5.1–15 mm, heavy at 15.1–30 mm, and severe above 30 mm [1]. These historical and thickness-based classifications provide useful quantitative context, but they should not be interpreted as interchangeable with the current operational FAA intensity definitions, because the consequences of icing also depend on aircraft configuration, exposure time, accretion location, and ice-protection capability [1,24,97]. As icing intensity increases or exceeds the capability of the aircraft and its protection systems, aircraft performance and operational margins can deteriorate, making icing classifications useful for communicating hazard level and supporting operational decision-making [24]. With the terminology for icing intensity established, the following section examines the principal aircraft-icing scenarios in which these conditions occur.

3.2. Icing Scenarios

Aircraft icing develops in several in-flight and ground scenarios. Major operational categories include structural, induction-system, and instrument icing [24]. Structural contamination may form in flight or accumulate on the ground as frost, snow, freezing precipitation, or refrozen water [23]. Ice-crystal icing is a distinct in-flight hazard in which high concentrations of ice crystals enter probes or gas-turbine engines and accrete under complex thermal and phase-change conditions [98].

3.2.1. Structural Icing

Structural icing develops when liquid moisture strikes aircraft surfaces cold enough for freezing. In flight, this generally requires visible liquid water, such as cloud droplets or rain, together with a local surface or impact temperature at or below 0 °C [23,24]. The local surface temperature can differ from the reported air temperature, so ice accretion may still occur when the surrounding air temperature is slightly above 0 °C [23].

Supercooled water droplets are central to structural ice accretion and commonly occur in clouds between 0 and −20 °C, although liquid water can persist at lower temperatures [23,24]. They form through cloud microphysical processes including condensation, collision–coalescence, and the melting of ice particles that subsequently enter a subfreezing layer. SLDs are commonly treated in aviation as droplets larger than approximately 50 μm in diameter; SLD environments include freezing drizzle and freezing rain [24]. Other reviews adopt a threshold of 100 μm [13], so SLD results should be compared using each study's stated size definition. Their greater inertia can extend impingement and runback beyond conventional leading-edge protection zones.

The extent to which SLD and smaller supercooled droplets contribute to aircraft icing depends on the surrounding cloud-phase and temperature conditions. Figure 2 summarizes the relationship among cloud phase, temperature, and the potential for structural icing from supercooled liquid water [99]. It does not assess the ice-crystal hazards discussed in Section 3.2.5, and its temperature bands are illustrative rather than universal cloud-phase boundaries. Within these icing environments, supercooled droplets can remain liquid below 0 °C until ice nucleation occurs [87,89]. As an aircraft encounters these droplets, their inertia causes a fraction of them to deviate from the airflow streamlines and impinge on leading-edge surfaces, as illustrated in Figure 3 [1,24]. After impact, the fraction of water that freezes immediately depends on the local heat balance. Heat released during freezing

must be removed through heat transfer to the surface and aerodynamic cooling associated with convective heat transfer to the surrounding airflow [1,21,24]. When this heat cannot be removed rapidly enough, some water remains liquid, spreads or runs back, and may freeze farther downstream [1,21,24]. Through continued droplet impingement and freezing, ice progressively accumulates and alters the local geometry of the aircraft surface [1,22,23].

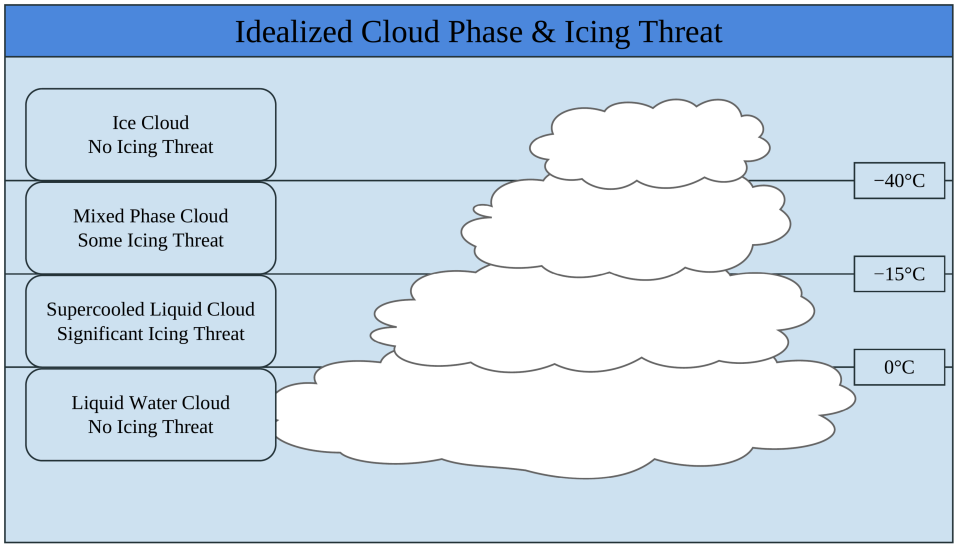

Figure 2. Idealized relationship between cloud phase, temperature, and potential icing threat. The schematic concerns structural icing from supercooled liquid water; fully glaciated clouds can still create ice-crystal hazards (Section 3.2.5). Temperature bands are indicative, not fixed phase boundaries.

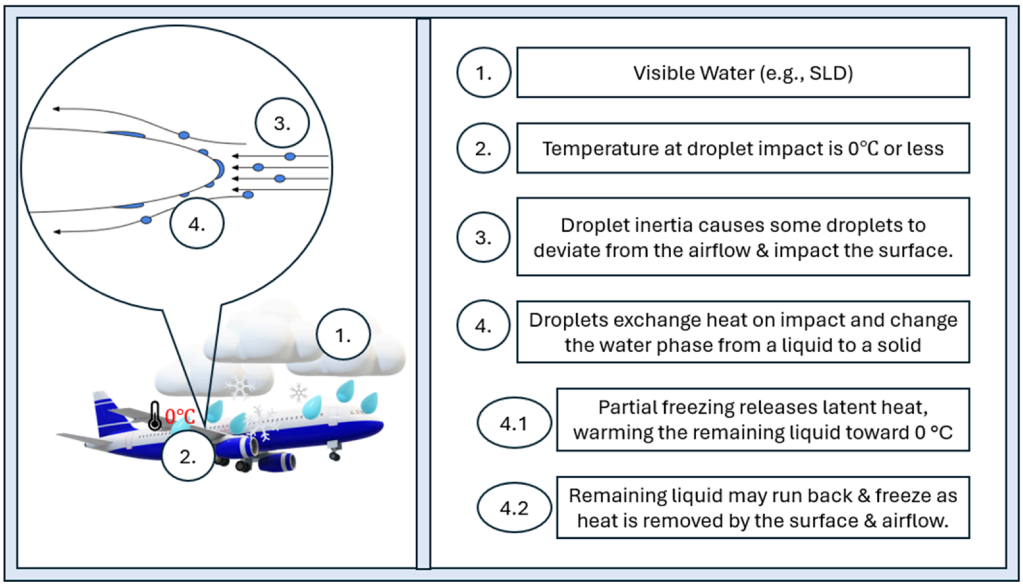

Figure 3. Schematic sequence of droplet impingement, heat exchange, freezing, and runback during aircraft ice accretion.

3.2.2. Ground Icing and Frost

Ground icing and frost are forms of frozen contamination that develop on aircraft before takeoff [24]. Frost, freezing precipitation, or snow can roughen lifting surfaces and reduce aerodynamic performance. Ice can also obstruct wheel wells, brake mechanisms, and flap hinges. Water splashed by wheels or driven by propellers may refreeze on the airframe, while contaminated runways and taxiways reduce traction and braking performance [1,23].

Frost can form on aircraft surfaces under clear, light-wind conditions when the surface becomes sufficiently cold. Although a thin frost layer may not substantially change the gross geometric profile of an airfoil, the resulting surface roughness can promote earlier airflow separation, reduce lift and increase stall speed [23]. Consequently, even relatively small amounts of frost can materially reduce takeoff and low-speed aerodynamic margins. Surface treatments that reduce wettability or ice adhesion may decrease frost or ice accumulation under some conditions, although their effectiveness depends on the surface and environmental conditions [23,100].

3.2.3. Induction-System Icing

Induction-system icing affects engine airflow, but the mechanism depends on the propulsion system. In carbureted piston engines, pressure reduction through the carburetor venturi, together with cooling from fuel vaporization, can lower the local air temperature enough for ice to form when moisture is present, including at ambient temperatures above 0 °C [23,24]. Gas-turbine engines do not experience carburetor icing; instead, ice can accrete in engine inlets, on inlet components, or within the compressor and engine core under suitable liquid-water, mixed-phase, or ice-crystal conditions [23,98,101]. In either propulsion system, ice accumulation can restrict or distort airflow and reduce available engine power or thrust [23,24,98,101]. When induction-system icing occurs during a broader icing encounter, the resulting propulsion degradation can compound the aerodynamic and instrumentation hazards associated with external ice accretion [23,24,98,101].

3.2.4. Instrument Icing

Instrument icing occurs when ice accumulates on exposed sensing components such as pitot tubes, static ports, and antennas [24]. Ice blockage of a pitot opening can corrupt the pressure signal used to determine indicated airspeed, while blockage of static ports can affect airspeed, altitude, and vertical-speed indications [23,102]. Ice accretion on antennas can also alter their aerodynamic loading and induce vibration, potentially degrading or damaging aircraft communication systems [23].

For context outside aviation, the European Space Agency (ESA) reported that a thin water-ice film on the Euclid telescope's optics reduced measured light and required controlled de-icing [103]. This is an example of instrument sensitivity to ice contamination; aircraft pitot–static icing involves different exposure and failure mechanisms, as described above.

3.2.5. Ice-Crystal Icing

Ice-crystal icing is associated with convective clouds containing high ice-water content and has been observed over a broad altitude range, including cruise altitudes above 39,000 ft (approximately 11.9 km) [98]. It affects gas-turbine compressor components, stagnation-pressure probes, and other heated aircraft parts [6,101]. Ice crystals may partially melt on warm surfaces, adhere, and then refreeze as local heat and mass transfer evolve, allowing accretion even where the local metal temperature initially exceeds 0 °C [98,104]. Consequences include thrust loss, engine damage or malfunction, unreliable flight-parameter indications, and autopilot disconnects. Particle fragmentation through the fan can further modify the size distribution of material entering the engine core [6].

3.3. Ice Accretion Types

In-flight structural ice accretion is generally divided into three categories: rime ice, glaze (clear) ice, and mixed ice. The type that forms is determined by the encounter conditions and, ultimately, by how much of the impinging water freezes on impact rather than remaining

liquid and moving across the surface before it freezes [1]. The characteristic accretion locations and shapes are compared schematically in Figure 4. The balance between freezing on impact and runback is quantified by the freezing fraction introduced in Section 2.3. Mixed ice is not necessarily greater in mass or more extensive in runback than either other type; those comparisons require matched exposure and thermal conditions.

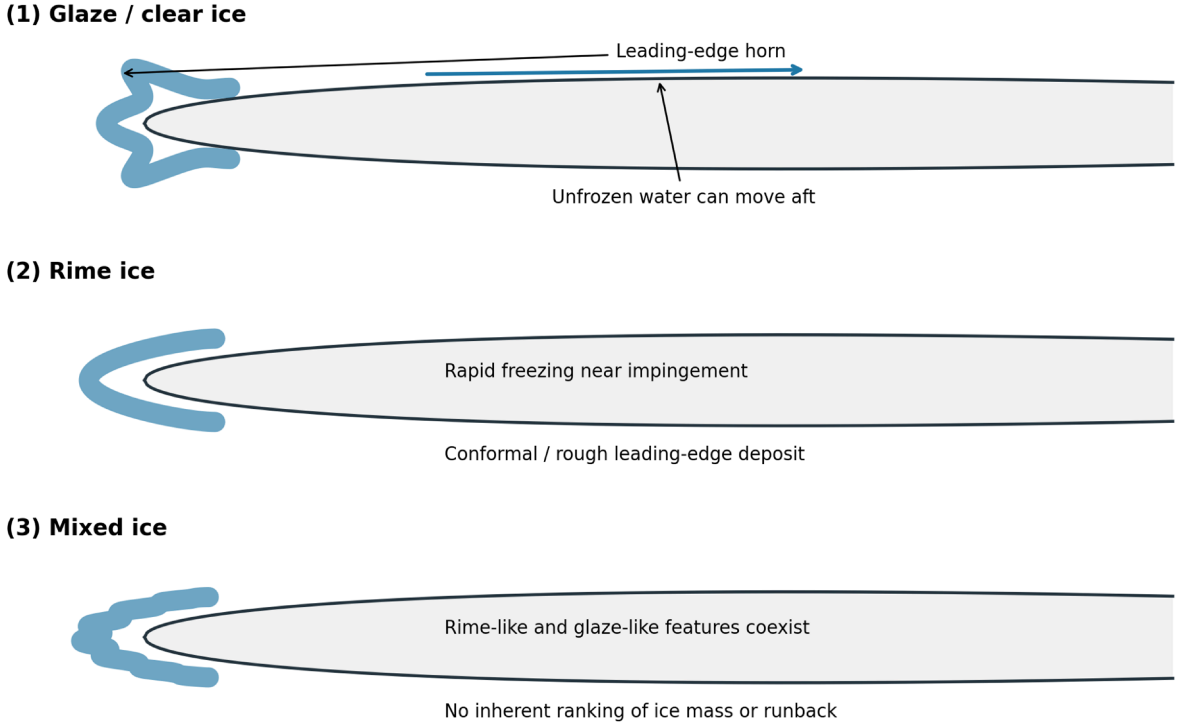

Figure 4. Conceptual leading-edge ice morphologies: (1) glaze/clear ice with representative horns and aft liquid transport, (2) rime ice with a more conformal leading-edge deposit, and (3) mixed ice with both types of features. The same airfoil outline is used in each panel. Ice outlines are illustrative; they do not predict relative accreted mass, encounter duration, or a universal ranking of runback distance.

3.3.1. Clear Ice

Clear or glaze ice forms when supercooled droplets do not freeze completely at the point of impact. Under conditions that favor a lower freezing fraction, part of the impinging water can remain liquid and spread or run downstream before solidifying, producing a relatively dense and often smooth or translucent accretion [1,23]. Nonuniform runback and freezing can also produce horn-like protrusions near the leading edge that strongly disturb the local airflow. The characteristic clear-ice accretion pattern is illustrated in Figure 4(1) [22,23,105]. Because of its density and strong adhesion, clear ice can be particularly difficult for ice-protection systems to remove [1,23].

3.3.2. Rime Ice

Rime ice forms when smaller, more strongly supercooled droplets freeze rapidly near the point of impact [1,23]. Because little liquid water remains available to spread downstream, the accretion is concentrated near the leading edge. Air trapped during rapid freezing gives rime ice its characteristic opaque, rough, and relatively low-density structure. The typical leading-edge accretion pattern is illustrated in Figure 4(2) [22,23,105]. Although rime ice is generally less dense and may be easier to remove than clear ice, its surface roughness can still produce substantial aerodynamic penalties [1,23].

3.3.3. Mixed Ice

Mixed ice develops when icing conditions support characteristics of both rapid freezing and liquid-water runback, producing an accretion with features of both rime and clear ice [1,23]. Variations in droplet size, liquid-water content, temperature, and other encounter conditions can cause these freezing behaviors to occur within the same accretion. The resulting ice is typically rough and irregular and may extend both near and downstream of the leading edge, as illustrated in Figure 4(3) [22,23,105]. Mixed ice can accumulate rapidly under some conditions and may be difficult for ice-protection systems to remove [1,23].

3.4. Icing Hazards

With the primary icing scenarios and accretion types established, the discussion now turns to aerodynamic, propulsion, instrumentation, and safety consequences. Icing exposure depends on temperature, liquid-water content, droplet-size distribution, encounter duration, and the spatial structure of the cloud [6]. Aircraft geometry and operating condition also affect collection efficiency; for example, angle of attack, α, changes the location and magnitude of droplet impingement [1,9].

3.4.1. Aerodynamic and Operational Impacts

Aircraft icing can degrade aerodynamic performance whenever ice roughness or accretion changes the effective shape of a lifting or propulsive surface. Typical consequences include reduced maximum lift, increased drag and weight, reduced propulsive efficiency or thrust, and increased stall speed. Ice can also shift the stall to a lower angle of attack; the magnitude of the penalty depends on accretion shape, location, surface roughness, and aircraft configuration [2,106]. Figure 5 summarizes these cumulative performance effects [107]. Instrument malfunctions and stability or control degradation further increase accident risk [1,2,22,108].

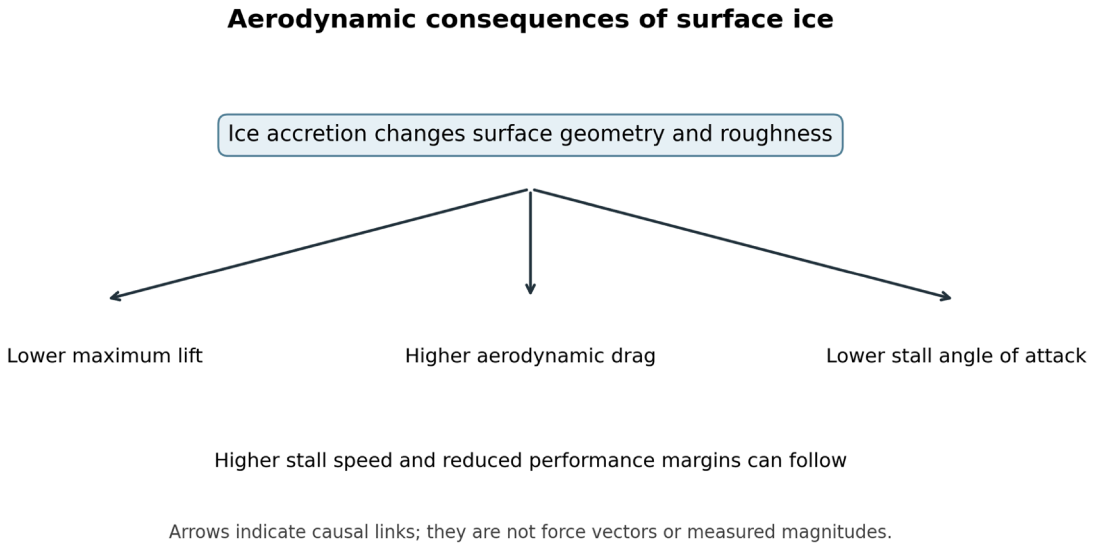

Figure 5. Qualitative consequences of ice-induced changes in airfoil geometry and roughness. All arrows denote causal links; none represents a force vector, a measured magnitude, or a quantitative comparison between clean and iced configurations.

Engine and instrument icing create additional operational hazards. Ice can restrict an engine inlet, distort inflow, reduce performance, or damage downstream components when shed ice is ingested [109,110]. Ice on pitot–static probes, stall-warning devices, or other sensors can produce erroneous indications or complete signal loss. These components are

therefore located, heated, or otherwise protected to reduce exposure and maintain reliable measurements [1].

3.4.2. Aircraft Icing Incidents

Accident statistics depend strongly on the dataset, period, aircraft category, and the distinction between a defining event and a contributing factor. Historical U.S. general-aviation data for 1990–2000 attributed 12% of weather-related accidents to icing, with most of those events occurring in flight [2]. Such figures should not be generalized to all commercial aviation or to later periods.

The National Transportation Safety Board (NTSB) U.S. Civil Aviation Accident Dashboard for 2008–2024 allows accidents to be filtered by defining event, including icing [111]. In this taxonomy, the icing category covers the accumulation of snow, ice, freezing precipitation, or frost on aircraft surfaces that adversely affects control or performance, whether in flight or on the ground; windscreen icing that restricts visibility; and ice accumulation on sensors, antennas, and other external surfaces, including those directly ahead of engine intakes [111,112]. Because the dashboard assigns a single defining event to each accident, an icing-filtered total does not capture every accident in which icing was a contributing factor.

Icing-related accidents may also be classified under another defining event. The Common Taxonomy Team recognizes occurrence categories in which snow, frost, freezing precipitation, contaminated surfaces, loss of control, or propulsion-system effects may be relevant [112]. For example, carburetor or induction icing may appear in a fuel-related or power-loss category rather than under icing itself. An NTSB safety alert reported that carburetor icing was a cause or factor in approximately 250 accidents from 2000 to 2011 and contributed to an average of two fatal accidents per year [113,114].

Accidents recorded under other defining events, such as loss of control, propulsion, runway excursion, or ground handling, should not be combined with the dashboard's defining-event count without examining the underlying investigations; different classifications answer different questions about the role of ice.

Dashboard categories and broader causal searches represent different populations. The FAA reports averages of approximately four accidents and five fatalities per year during 2008–2021 for accidents in which structural in-flight icing was identified as a cause or factor [115]. These U.S. statistics are not a worldwide total for all icing mechanisms, and the rounded annual averages should not be converted into an exact fatality count. Pitot-probe obstruction is an instrument-icing mechanism. The BEA report on Air France flight 447, which involved 228 fatalities, describes unreliable airspeed associated with temporary pitot obstruction in an ice-crystal environment and a subsequent loss-of-control sequence [116]. It illustrates a different mechanism and reporting population, not an inconsistency with the FAA structural-icing statistic.

4. Ice-Protection and Mitigation Strategies

Ice protection uses physical mechanisms to prevent/delay accretion or remove existing ice. Supplied heat, structural actuation, and delivered fluids are active system functions; passive coatings modify water retention or ice adhesion. A pumped fluid system must not be classed as entirely passive just because its fluid acts chemically. Forecasting, sensing, and data-assisted control facilitate these functions and do not remove ice in isolation [108,117,118]. In the proprietary TKS in-flight ice-protection system, a pump meters glycol-based fluid through porous leading-edge panels; the fluid mixes with impinging water to lower the mixture's freezing point and is carried aft over the surface [86]. Table 2 separates operating principle, development status, and the evidence needed for application.

Icing wind tunnels provide controlled and repeatable environments for studying accretion physics and evaluating protection systems before flight testing. Their spray calibration, thermal control, flow quality, test-section geometry, and instrumentation make them complex and costly facilities. Bansmer et al. describe the design and commissioning of the Braunschweig Icing Wind Tunnel, including its drive, cooling, settling, spray, nozzle, wall, corrosion-protection, and measurement systems [6]. Such facilities are particularly important for evaluating lightweight passive surfaces and hybrid concepts under representative droplet-size, liquid-water-content, velocity, and temperature conditions [119]. Table 2 compares protection mechanisms and facilitating technologies, and Figure 6 distinguishes physical protection functions from facilitating measurement, diagnosis, and control.

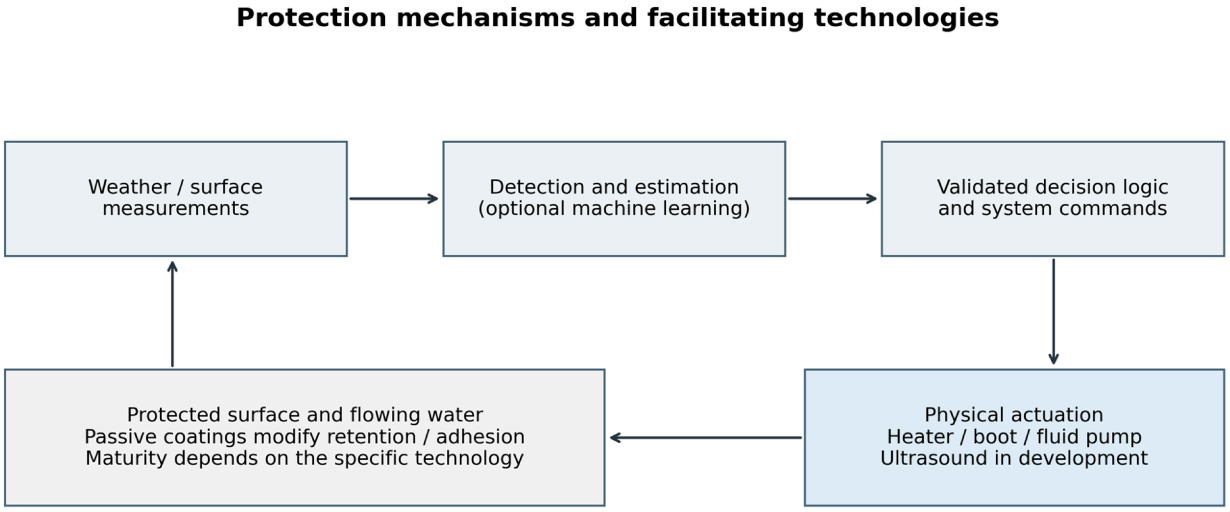

Figure 6. Distinction between physical ice-protection functions and facilitating measurement, diagnosis, and control. Machine learning can support estimation and commands, while heaters, boots, fluid delivery, or other physical mechanisms provide protection. Ultrasound and passive-surface implementations require application-specific validation; the diagram does not imply equal maturity.

Table 2. Protection mechanisms and facilitating technologies, with development status. The status describes the cited class or installation; it is not a numerical technology-readiness level and does not imply approval for every aircraft or icing envelope. AI, artificial intelligence; ML, machine learning.

Technology/Role	Physical Mechanism/Setting	Development Status in Cited Evidence	Main Limits and Validation Needs
Thermal protection	Bleed-air or electrothermal heat prevents freezing or melts ice.	Established operational aircraft installations [108,117,120,121].	Energy and thermal integration; protected area; wet runback and downstream refreezing.
Pneumatic boots	Cyclic deformation fractures and sheds an existing ice layer.	Established operational installations; timing follows aircraft procedures [108,117].	Ice thickness/adhesion, structural integration, actuation, and shed-ice consequences.
Electro-impulse	Electromagnetic impulse drives transient skin deformation.	Aircraft-oriented engineering demonstrations; maturity is installation-specific [122].	Fatigue, electromagnetic integration, load transmission, and reliable shedding.

Table 2. *Cont.*

Technology/Role	Physical Mechanism/Setting	Development Status in Cited Evidence	Main Limits and Validation Needs
Ground fluids/in-flight TKS	Freezing-point depression; TKS adds powered metering through porous panels.	Ground practice and aircraft-specific approved in-flight installations [86,108].	Coverage, fluid endurance, delivery/pump availability, and approved icing envelope.
Ultrasonic de-icing	Piezoelectric excitation creates ice–surface stresses.	Research, component demonstrations, and aircraft-level analyses in cited work [123,124].	Mode coverage, transducer bonding, fatigue, energy at equal duty, and system reliability.
Passive icephobic surfaces	Modify retention, nucleation, runback, or ice adhesion.	Predominantly material/coupon and representative-airfoil studies; application-specific [74,105,119,125].	Repeated impacts, frost/condensation, wear, contamination, and sustained protection.
Sensing/AI decision support	Estimates ice state or protection need; commands a separate physical system.	Operational sensing exists; cited ML concepts are research demonstrations [126–131].	False alarms, missed detections, domain shift, independent validation, and fail-safe control.

4.1. Thermal Methods

Thermal systems can provide both anti-icing and de-icing. They prevent accretion by maintaining a protected surface above the local freezing threshold or remove existing ice by melting the interface or the full accretion. Heat may be supplied by engine compressor bleed air or by electrical heaters embedded beneath the surface. Electrothermal protection is commonly applied to windshields, propellers, and air-data probes. Operating strategies include continuous anti-icing and cyclic or intermittent de-icing [105,108,117,120,121].

Thermal ice protection is established in operational aircraft, although each installation is approved for a specified envelope. Running-wet operation, in which water remains liquid over the heated region, must account for its subsequent transport and potential refreezing downstream [40,108,117].

4.2. Mechanical Methods

Mechanical de-icing removes accumulated ice by deforming or accelerating the protected surface. Pneumatic boots, typically installed on leading edges, inflate cyclically to fracture and shed an ice layer. Electro-impulse systems rapidly discharge stored electrical energy through coils beneath a conductive skin; the resulting electromagnetic load creates a transient structural deformation that fractures or debonds the ice [108,117,122]. Performance depends on ice thickness, adhesion, structural stiffness, and actuation timing.

Pneumatic boots have established operational use; that status should not automatically be assigned to every mechanical or electromagnetic concept. The electro-impulse evidence cited here concerns a particular engineering implementation, whose integration and reliability must be assessed separately [122].

4.3. Chemical and Fluid-Based Methods

Chemical fluids can remove or delay ice by depressing the freezing point and altering the interfacial liquid layer. Ground de-icing commonly uses heated glycol–water mixtures; some ground anti-icing formulations use thickeners to extend surface residence before

takeoff [108]. Fluid-based protection is also used in flight. Aircraft-specific approved TKS installations provide in-flight fluid protection [86]. Their performance depends on fluid flow and coverage, the finite onboard fluid supply, pump availability, and the approved operating envelope. The freezing-point depression is coupled with powered fluid delivery.

4.4. Icephobic, Superhydrophobic, and Mixed-Wettability Surfaces

Physicochemical approaches modify the surface to reduce liquid retention, delay freezing, or lower ice adhesion. Surfaces are commonly described as icephobic when their ice adhesion strength is below approximately 100 kPa, well below the values typically measured on bare structural metals [52,70]. Hydrophobic, superhydrophobic, and lubricant-infused coatings can reduce accretion under selected conditions, but durability, contamination, erosion, and lubricant depletion remain important limitations [108,125]. Combining a passive coating with thermal, mechanical, or ultrasonic protection may reduce active-system energy demand, although each pairing requires flight-relevant durability and system-level validation.

Superhydrophobic surfaces use hierarchical texture and low-surface-energy chemistry to reduce water retention and liquid–solid contact. Natural examples such as lotus leaves and some insect wings motivate artificial, self-cleaning water-repellent surfaces [74,132–134]. Under favorable impact and thermal conditions, these surfaces can promote rebound or shedding, delay freezing, and reduce ice adhesion [105,119]. Their performance is not universal: high-speed impact, condensation, frost, damage, and contamination can suppress the non-wetting state.

Passive surface studies require outcome-specific interpretation. Repelling a drop before it freezes reduces retained water; reducing adhesion after freezing assists subsequent removal. These are not equivalent demonstrations of standalone protection. The reported response can change with repeated impacts, frost, wetting-state transitions, erosion, contamination, and thermal cycling [9,105,119]. Representative-airfoil and durability tests are required to establish whether a coating reduces the demand on an active system over sustained icing exposure.

Mixed-wettability surfaces combine regions with different contact angles to direct, collect, or shed droplets [132]. Natural analogues use patterned hydrophilic and hydrophobic regions to guide water, motivating engineered surfaces that localize liquid away from critical zones [132,135]. Proposed anti-icing functions include directing droplets toward shedding locations, delaying nucleation, and controlling spreading [74,132,136]. These surfaces may also complement active systems by reducing the liquid or ice load that the active protection must manage.

4.5. Ultrasonic Methods

Ultrasonic de-icing uses piezoelectric excitation to develop stresses that can fracture or debond ice. Its development should be distinguished from established pneumatic boots and thermal installations. The cited literature includes laboratory/component demonstrations and aircraft-level benefit analyses, not a basis for claiming routine fleet-wide certification or interchangeability with existing systems [117,123,124]. Performance depends on structural modes, geometry, excitation frequency, transducer placement and bonding, ice thickness, fatigue, and the fate of shed ice. Ultrasonic detection and thickness measurement are separate demonstrated functions and do not by themselves establish de-icing capability [137–139]. Energy comparisons require the same protected area, icing exposure, operating duration, and removal criterion.

4.6. Forecasting, Sensing, and Data-Assisted Decision Support

Mitigation also includes forecasting and detection tools that allow crews or protection systems to respond before accretion becomes hazardous. Operational icing products characterize the probability and expected intensity of icing and support route planning. U.S. transport-aircraft certification distinguishes conventional icing envelopes in Appendix C from supercooled-large-droplet environments in Appendix O of Part 25 of Title 14 of the Code of Federal Regulations (14 CFR) [140]; forecasting and detection products that distinguish these regimes are therefore operationally important. Continued work also emphasizes automated diagnosis and forecasts that distinguish icing regimes and provide timely information to pilots, dispatchers, and meteorologists [115].

Machine learning, a subset of artificial intelligence (AI), is used to interpret measurements or support protection decisions, including image-based ground de-icing support and wing-icing detection [126,127]. In the graphene-associated system studied by Farina et al. [128], thermocouples capture temperature signatures of freezing and electrical current through graphene strips supplies resistive heating. The algorithms classify thermal patterns associated with ice/no-ice states; graphene is a component of the integrated sensing/heating architecture, not an intrinsic requirement for machine learning. The study reports false positives for overlapping unsupervised clusters. Transfer beyond the test setup therefore requires independent validation across temperature, airflow, contamination, and sensor drift. Any commanded ice removal is performed by the heater or another actuator, not by the classifier.

Machine learning has also been used to estimate anti-icing surface temperature and to evaluate icing severity from variables such as liquid-water content, droplet diameter, exposure time, accreted area, and maximum ice thickness [129,130]. Broader aviation applications include predictive maintenance and weather-informed operational decision support [131]. These systems remain at an early stage for safety-critical icing control; certification will require interpretable performance limits, robust failure handling, and evidence that models generalize beyond their development datasets.

4.7. Comparative Assessment and Evidence Gaps

Protection methods must be compared at the same level of evidence. Operational thermal, pneumatic, and aircraft-specific fluid systems have installation and operating constraints; favorable drop tests on a passive surface and benefit calculations for an ultrasonic concept do not establish equivalent aircraft capability [11–13,108,117,119,122–125]. Sensing and AI should be compared through detection delay, false alarms, missed detections, and control reliability. Physical protection should be compared through retained water/ice, protected area, runback, removal completeness, energy or fluid use, and sustained performance. This distinction is the central system-level outcome of the present synthesis; it supplements the detailed SLD-process emphasis of Guo et al. [13].

The evidence is not sufficiently uniform for a defensible universal ranking of protection methods. A useful test record includes the incident size distribution, local normal/tangential impact speeds, airflow, liquid and surface temperatures, *LWC*, geometry, surface age/roughness, exposure duration, and measurement definitions. Report repeatability and sensor uncertainty separately from numerical discretization error and model–experiment discrepancy. For surface water, measure film/rivulet velocity, wetted coverage, downstream freezing location, and retained mass. For an integrated system, also report protected area, energy/fluid consumption, failure behavior, and post-test surface condition. Matching Weber number alone does not match aerodynamic breakup, heat balance, nucleation statistics, or runback.

5. Conclusions, Limitations, and Future Directions

Aircraft icing emerges from a coupled sequence: droplets are transported by airflow, deviate from streamlines and impinge on aircraft surfaces, spread or recoil according to impact and surface conditions, exchange heat with the surface and surrounding flow, nucleate, and either freeze locally or run back before solidifying. This sequence provides a physical framework for interpreting clear, rime, and mixed ice and for connecting atmospheric conditions to aerodynamic, propulsion, sensing, and operational hazards. The freezing fraction provides the quantitative bridge between droplet-scale freezing behavior and accretion morphology.

Established thermal, pneumatic, and fluid-based protection should be distinguished from developing ultrasonic and passive-surface implementations. Ground fluids and in-flight TKS systems have different delivery and endurance constraints. Passive surfaces may reduce retained water or adhesion, but their contribution must be demonstrated under sustained representative exposure. Sensing, forecasting, and machine learning facilitate diagnosis and control; physical actuators and supplied energy or fluids perform the protection function.

The main limitations are the narrative selection of sources and the nonuniform conditions and evidence quality across studies. The targeted searches described in Section Review Approach do not establish exhaustive coverage. Isolated-drop, moving-airfoil, icing-tunnel, and integrated-system studies answer different questions, so their outcomes cannot be pooled into a single performance ranking. These limitations motivate the condition and uncertainty fields in Table 1 and the development-status distinctions in Table 2.

Future work should connect the measured local droplet state at impact to surface-water transport and the location of freezing. Experiments should distinguish breakup before impact from splashing after contact and should validate coupled models against water-retention and runback measurements as well as ice shape. Surface concepts need repeated-impact and durability evidence; ultrasonic concepts need structural integration and reliability assessment; diagnostic algorithms need independent data and fail-safe integration. These priorities connect the mechanism review to the selection and validation of aircraft protection systems.

Author Contributions: Conceptualization, S.M.; supervision, S.M.; writing—original draft preparation, M.T. and T.T.; writing—review and editing, S.M. All authors have read and agreed to the published version of the manuscript.

Funding: This research received no external funding.

Institutional Review Board Statement: Not applicable.

Informed Consent Statement: Not applicable.

Data Availability Statement: No new data were created or analyzed in this study. Data sharing is not applicable to this article.

Acknowledgments: The authors acknowledge the support of the Honors Program and the Undergraduate Research Opportunity Program at California State University Long Beach. During the preparation of this manuscript, the authors used ChatGPT (GPT-5.6 Luna) for language editing. The authors have reviewed and edited the output and take full responsibility for the content of this publication.

Conflicts of Interest: The authors declare no conflicts of interest.

Nomenclature

J	Ice nucleation rate	We	Weber number
K	Kinetic prefactor	ρ	Liquid density
ΔG	Free-energy barrier	σ	Liquid surface tension
k_B	Boltzmann constant	U	Impact velocity
T	Absolute temperature	D	Droplet diameter
θ	Static contact angle	α	Angle of attack
Re	Reynolds number	Oh	Ohnesorge number
K_s	Splashing parameter	μ	Liquid dynamic viscosity
β	Local collection efficiency	LWC	Liquid water content
V_∞	Free-stream velocity	n_0	Freezing fraction
$\dot{m}_{imp}$	Impinging water mass flux	$\dot{m}_{fr}$	Freezing water mass flux
$\dot{m}_{\mathrm{rb,in}}$	Incoming runback mass flux		
q	Film volume flux per unit span	h	Local film thickness
s	Surface coordinate	τ_a	Aerodynamic shear stress
p	Liquid pressure	g_t	Tangential gravity component
θ_i	Ice-embryo contact angle	$f(\theta_i)$	Nucleation geometric factor
ρ_g	Gas density	$u_g - u_d$	Gas–droplet slip velocity

Abbreviations

The following abbreviations are used in this manuscript:

AI	artificial intelligence
CFR	Code of Federal Regulations
CIRA	Italian Aerospace Research Centre
ESA	European Space Agency
FAA	Federal Aviation Administration
NASA	National Aeronautics and Space Administration
NTSB	National Transportation Safety Board
SLD	supercooled large droplet
NTRS	NASA Technical Reports Server
VOF	volume of fluid
SD	standard deviation
BEA	Bureau d'Enquêtes et d'Analyses pour la Sécurité de l'Aviation Civile
TKS	porous-panel fluid-based ice-protection system (trade name)
ML	machine learning
NR-E	quantitative uncertainty not extracted from the inspected source
MVD	median volume diameter

References

1. Cao, Y.; Tan, W.; Wu, Z. Aircraft Icing: An Ongoing Threat to Aviation Safety. *Aerosp. Sci. Technol.* **2018**, *75*, 353–385. [CrossRef]
2. Cao, Y.; Wu, Z.; Su, Y.; Xu, Z. Aircraft Flight Characteristics in Icing Conditions. *Prog. Aerosp. Sci.* **2015**, *74*, 62–80. [CrossRef]
3. Guardone, A.; Bellosta, T.; Donizetti, A.; Gallia, M. Aircraft Icing: Modeling and Simulation. *Annu. Rev. Fluid Mech.* **2026**, *58*, 139–165. [CrossRef]
4. Moghtadernejad, S.; Tembely, M.; Jadidi, M.; Esmail, N.; Dolatabadi, A. Shear Driven Droplet Shedding and Coalescence on a Superhydrophobic Surface. *Phys. Fluids* **2015**, *27*, 032106. [CrossRef]
5. Fuller, M.P.; Fuller, A.M.; Kaniouras, S.; Christophers, J.; Fredericks, T. The Freezing Characteristics of Wheat at Ear Emergence. *Eur. J. Agron.* **2007**, *26*, 435–441. [CrossRef]
6. Bansmer, S.E.; Baumert, A.; Sattler, S.; Knop, I.; Leroy, D.; Schwarzenboeck, A.; Jurkat-Witschas, T.; Voigt, C.; Pervier, H.; Esposito, B. Design, Construction and Commissioning of the Braunschweig Icing Wind Tunnel. *Atmos. Meas. Tech.* **2018**, *11*, 3221–3249. [CrossRef]
7. Nasr, M.R.; Fauchoux, M.; Besant, R.W.; Simonson, C.J. A Review of Frosting in Air-to-Air Energy Exchangers. *Renew. Sustain. Energy Rev.* **2014**, *30*, 538–554. [CrossRef]
8. Alsabagh, A.S.Y.; Tiu, W.; Xu, Y.; Virk, M.S. A Review of the Effects of Ice Accretion on the Structural Behavior of Wind Turbines. *Wind Eng.* **2013**, *37*, 59–70. [CrossRef]
9. Potapczuk, M.G. Aircraft Icing Research at NASA Glenn Research Center. *J. Aerosp. Eng.* **2013**, *26*, 260–276. [CrossRef]

10. Ratvasky, T.P.; Barnhart, B.P.; Lee, S. Current Methods Modeling and Simulating Icing Effects on Aircraft Performance, Stability, Control. *J. Aircr.* **2010**, *47*, 201–211. [CrossRef]
11. Cui, Y.; Chen, W.; Dai, N.; Han, C. Integrated Technologies for Anti-Deicing Functions and Structures of Aircraft: Current Status and Development Trends. *Aerospace* **2024**, *11*, 821. [CrossRef]
12. Rekuviene, R.; Saeidiharzand, S.; Mažeika, L.; Samaitis, V.; Jankauskas, A.; Sadaghiani, A.K.; Gharib, G.; Muganlı, Z.; Koşar, A. A Review on Passive and Active Anti-Icing and De-Icing Technologies. *Appl. Therm. Eng.* **2024**, *250*, 123474. [CrossRef]
13. Guo, Y.; Liu, Y.; Sussman, M.; Hu, H.; Lian, Y. Recent Developments in Supercooled Large Droplet Research: Impact, Splashing, Surface Water Dynamics, and Ice Accretion. *Fluids* **2026**, *11*, 162. [CrossRef]
14. Fang, W.-Z.; Zhu, F.; Zhu, L.; Tao, W.-Q.; Yang, C. Self-Peeling of Frozen Water Droplets upon Impacting a Cold Surface. *Commun. Phys.* **2022**, *5*, 51. [CrossRef]
15. Gorin, B.; Bonn, D.; Kellay, H. Droplet Impacts on Cold Surfaces. *J. Fluid Mech.* **2022**, *944*, A23. [CrossRef]
16. Zhang, X.; Liu, X.; Wu, X.; Min, J. Impacting-Freezing Dynamics of a Supercooled Water Droplet on a Cold Surface: Rebound and Adhesion. *Int. J. Heat Mass Transf.* **2020**, *158*, 119997. [CrossRef]
17. Hosseini, S.R.; Moghimi, M.; Nouri, N.M. On the Role of Surface Morphology in Impacting-Freezing Dynamics of Supercooled Droplets. *Sci. Rep.* **2024**, *14*, 12585. [CrossRef] [PubMed]
18. Worthington, A.M. *A Study of Splashes*; Longmans, Green, and Co.: London, UK, 1908.
19. Worthington, A.M.; Clifton, R.B. XXVIII. On the Forms Assumed by Drops of Liquids Falling Vertically on a Horizontal Plate. *Proc. R. Soc. Lond.* **1877**, *25*, 261–272. [CrossRef]
20. Roisman, I.V.; Tropea, C. Wetting and Icing of Surfaces. *Curr. Opin. Colloid Interface Sci.* **2021**, *53*, 101400. [CrossRef]
21. Makkonen, L. Models for the Growth of Rime, Glaze, Icicles and Wet Snow on Structures. *Philos. Trans. R. Soc. A* **2000**, *358*, 2913–2939. [CrossRef]
22. Cebeci, T.; Kafyeke, F. Aircraft Icing. *Annu. Rev. Fluid Mech.* **2003**, *35*, 11–21. [CrossRef]
23. Federal Aviation Administration. *AC 00-6A, Aviation Weather for Pilots and Flight Operations Personnel*; Chapter 10: Icing; FAA: Washington, DC, USA, 1975.
24. Federal Aviation Administration. *Aviation Weather Handbook*; FAA: Washington, DC, USA, 2026.
25. Rioboo, R.; Tropea, C.; Marengo, M. Outcomes from a Drop Impact on Solid Surfaces. *At. Sprays* **2001**, *11*, 12. [CrossRef]
26. Liang, G.; Yang, Y.; Guo, Y.; Zhen, N.; Shen, S. Rebound and Spreading during a Drop Impact on Wetted Cylinders. *Exp. Therm. Fluid Sci.* **2014**, *52*, 97–103. [CrossRef]
27. Bange, P.G.; Patil, N.D.; Bhardwaj, R. Impact Dynamics of a Droplet on a Heated Surface. In Proceedings of the 5th International Conference of Fluid Flow, Heat and Mass Transfer (FFHMT '18), Niagara Falls, ON, Canada, 7–9 June 2018; pp. 7–9.
28. Ding, B.; Wang, H.; Zhu, X.; Chen, R.; Liao, Q. How Supercooled Superhydrophobic Surfaces Affect Dynamic Behaviors of Impacting Water Droplets? *Int. J. Heat Mass Transf.* **2018**, *124*, 1025–1032. [CrossRef]
29. Josserand, C.; Thoroddsen, S.T. Drop Impact on a Solid Surface. *Annu. Rev. Fluid Mech.* **2016**, *48*, 365–391. [CrossRef]
30. Rein, M. Phenomena of Liquid Drop Impact on Solid and Liquid Surfaces. *Fluid Dyn. Res.* **1993**, *12*, 61–93. [CrossRef]
31. Yarin, A.L. Drop Impact Dynamics: Splashing, Spreading, Receding, Bouncing. *Annu. Rev. Fluid Mech.* **2006**, *38*, 159–192. [CrossRef]
32. Marengo, M.; Antonini, C.; Roisman, I.V.; Tropea, C. Drop Collisions with Simple and Complex Surfaces. *Curr. Opin. Colloid Interface Sci.* **2011**, *16*, 292–302. [CrossRef]
33. Moghtadernejad, S.; Lee, C.; Jadidi, M. An Introduction of Droplet Impact Dynamics to Engineering Students. *Fluids* **2020**, *5*, 107. [CrossRef]
34. Zhao, P.; Hargrave, G.K.; Versteeg, H.K.; Garner, C.P.; Reid, B.A.; Long, E.J.; Zhao, H. The Dynamics of Droplet Impact on a Heated Porous Surface. *Chem. Eng. Sci.* **2018**, *190*, 232–247. [CrossRef]
35. Zhang, R.; Hao, P.; Zhang, X.; He, F. Supercooled Water Droplet Impact on Superhydrophobic Surfaces with Various Roughness and Temperature. *Int. J. Heat Mass Transf.* **2018**, *122*, 395–402. [CrossRef]
36. Burzynski, D.A.; Bansmer, S.E. Droplet Splashing on Thin Moving Films at High Weber Numbers. *Int. J. Multiph. Flow* **2018**, *101*, 202–211. [CrossRef]
37. Wang, J.; Guo, R.; Zhao, N.; Zhu, C. An Experimental Investigation of the Effect of a Supercooled Large Droplet Impingement on Freezing Behaviour. *Aeronaut. J.* **2025**, *129*, 2556–2574. [CrossRef]
38. Gao, X.-L.; Luo, K.; Wu, J.; Yi, H.-L. Effects of Frosting on the Impacting Droplets Spreading and Freezing on Subcooled Surfaces. *Int. J. Heat Mass Transf.* **2024**, *221*, 125079. [CrossRef]
39. Khojasteh, D.; Kazerooni, M.; Salarian, S.; Kamali, R. Droplet Impact on Superhydrophobic Surfaces: A Review of Recent Developments. *J. Ind. Eng. Chem.* **2016**, *42*, 1–14. [CrossRef]
40. Gent, R.W.; Dart, N.P.; Cansdale, J.T. Aircraft Icing. *Philos. Trans. R. Soc. A* **2000**, *358*, 2873–2911. [CrossRef]
41. Vargas, M.; Sor, S.; García-Magariño, A. *Mechanism of Water Droplet Breakup Near the Leading Edge of an Airfoil; NASA/TM-2012-217704*; AIAA Paper 2012-3129; NASA Glenn Research Center: Cleveland, OH, USA, 2012.

42. Pan, Y.; Shi, K.; Duan, X.; Naterer, G.F. Experimental Investigation of Water Droplet Impact and Freezing on Micropatterned Stainless Steel Surfaces with Varying Wettabilities. *Int. J. Heat Mass Transf.* **2019**, *129*, 953–964. [CrossRef]
43. Rajesh, R.S.; Naveen, P.T.; Krishnakumar, K.; Ranjith, S.K. Dynamics of Single Droplet Impact on Cylindrically-Curved Superheated Surfaces. *Exp. Therm. Fluid Sci.* **2019**, *101*, 251–262. [CrossRef]
44. Wang, X.; Wang, Y.; Yang, G.; Liu, S.; Kosonen, R.; Li, Q.; Yang, Z.; Yang, X.; Sun, X.; Wang, S. Study on Fluid Flow and Heat Transfer Characteristics of Supercooled Large Droplet Impingement on Wing Surfaces. *J. Therm. Anal. Calorim.* **2026**, *151*, 4471–4495. [CrossRef]
45. Mohammadi, M.; Tembely, M.; Dolatabadi, A. Supercooled Water Droplet Impacting Superhydrophobic Surfaces in the Presence of Cold Air Flow. *Appl. Sci.* **2017**, *7*, 130. [CrossRef]
46. Mundo, C.; Sommerfeld, M.; Tropea, C. Droplet–Wall Collisions: Experimental Studies of the Deformation and Breakup Process. *Int. J. Multiph. Flow* **1995**, *21*, 151–173. [CrossRef]
47. Moghtadernejad, S.; Jadidi, M.; Tembely, M.; Esmail, N.; Dolatabadi, A. Concurrent Droplet Coalescence and Solidification on Surfaces with Various Wettabilities. *J. Fluids Eng.* **2015**, *137*, 071302. [CrossRef]
48. Wang, J.; Hu, H.; He, P.; Hu, H. A Machine Learning Study to Predict Wind-Driven Water Runback Characteristics. *Phys. Fluids* **2023**, *35*, 102104. [CrossRef]
49. Jung, S.; Tiwari, M.K.; Doan, N.V.; Poulikakos, D. Mechanism of Supercooled Droplet Freezing on Surfaces. *Nat. Commun.* **2012**, *3*, 615. [CrossRef] [PubMed]
50. Chaudhary, G.; Li, R. Freezing of Water Droplets on Solid Surfaces: An Experimental and Numerical Study. *Exp. Therm. Fluid Sci.* **2014**, *57*, 86–93. [CrossRef]
51. Li, H.; Roisman, I.V.; Tropea, C. Influence of Solidification on the Impact of Supercooled Water Drops onto Cold Surfaces. *Exp. Fluids* **2015**, *56*, 133. [CrossRef]
52. Kreder, M.J.; Alvarenga, J.; Kim, P.; Aizenberg, J. Design of Anti-Icing Surfaces: Smooth, Textured or Slippery? *Nat. Rev. Mater.* **2016**, *1*, 15003. [CrossRef]
53. Bird, J.C.; Dhiman, R.; Kwon, H.-M.; Varanasi, K.K. Reducing the Contact Time of a Bouncing Drop. *Nature* **2013**, *503*, 385–388. [CrossRef] [PubMed]
54. Kim, S.H.; Jiang, Y.; Kim, H. Droplet Impact and LFP on Wettability and Nanostructured Surface. *Exp. Therm. Fluid Sci.* **2018**, *99*, 85–93. [CrossRef]
55. Walker, J. Boiling and the Leidenfrost Effect. In *Fundamentals of Physics*; Wiley: Hoboken, NJ, USA, 2010; p. E10-1.
56. Chen, H.; Cheng, W.; Peng, Y.; Jiang, L. Dynamic Leidenfrost Temperature Increase of Impacting Droplets Containing High-Alcohol Surfactant. *Int. J. Heat Mass Transf.* **2018**, *118*, 1160–1168. [CrossRef]
57. Chu, K.-H.; Xiao, R.; Wang, E.N. Uni-Directional Liquid Spreading on Asymmetric Nanostructured Surfaces. *Nat. Mater.* **2010**, *9*, 413–417. [CrossRef] [PubMed]
58. Kusumaatmaja, H.; Vrancken, R.J.; Bastiaansen, C.W.M.; Yeomans, J.M. Anisotropic Drop Morphologies on Corrugated Surfaces. *Langmuir* **2008**, *24*, 7299–7308. [CrossRef] [PubMed]
59. Chung, J.Y.; Youngblood, J.P.; Stafford, C.M. Anisotropic Wetting on Tunable Micro-Wrinkled Surfaces. *Soft Matter* **2007**, *3*, 1163–1169. [CrossRef] [PubMed]
60. Chen, Y.; He, B.; Lee, J.; Patankar, N.A. Anisotropy in the Wetting of Rough Surfaces. *J. Colloid Interface Sci.* **2005**, *281*, 458–464. [CrossRef] [PubMed]
61. Zhang, F.; Low, H.Y. Anisotropic Wettability on Imprinted Hierarchical Structures. *Langmuir* **2007**, *23*, 7793–7798. [CrossRef] [PubMed]
62. Drelich, J.; Wilbur, J.L.; Miller, J.D.; Whitesides, G.M. Contact Angles for Liquid Drops at a Model Heterogeneous Surface Consisting of Alternating and Parallel Hydrophobic/Hydrophilic Strips. *Langmuir* **1996**, *12*, 1913–1922. [CrossRef]
63. Boinovich, L.; Emelyanenko, A.M.; Korolev, V.V.; Pashinin, A.S. Effect of Wettability on Sessile Drop Freezing: When Superhydrophobicity Stimulates an Extreme Freezing Delay. *Langmuir* **2014**, *30*, 1659–1668. [CrossRef] [PubMed]
64. Antonini, C.; Innocenti, M.; Horn, T.; Marengo, M.; Amirfazli, A. Understanding the Effect of Superhydrophobic Coatings on Energy Reduction in Anti-Icing Systems. *Cold Reg. Sci. Technol.* **2011**, *67*, 58–67. [CrossRef]
65. Yoshimitsu, Z.; Nakajima, A.; Watanabe, T.; Hashimoto, K. Effects of Surface Structure on the Hydrophobicity and Sliding Behavior of Water Droplets. *Langmuir* **2002**, *18*, 5818–5822. [CrossRef]
66. Mishchenko, L.; Hatton, B.; Bahadur, V.; Taylor, J.A.; Krupenkin, T.; Aizenberg, J. Design of Ice-Free Nanostructured Surfaces Based on Repulsion of Impacting Water Droplets. *ACS Nano* **2010**, *4*, 7699–7707. [CrossRef] [PubMed]
67. Hejazi, V.; Sobolev, K.; Nosonovsky, M. From Superhydrophobicity to Icephobicity: Forces and Interaction Analysis. *Sci. Rep.* **2013**, *3*, 2194. [CrossRef] [PubMed]
68. Bahadur, V.; Mishchenko, L.; Hatton, B.; Taylor, J.A.; Aizenberg, J.; Krupenkin, T. Predictive Model for Ice Formation on Superhydrophobic Surfaces. *Langmuir* **2011**, *27*, 14143–14150. [CrossRef] [PubMed]

69. Kulinich, S.A.; Farhadi, S.; Nose, K.; Du, X.W. Superhydrophobic Surfaces: Are They Really Ice-Repellent? *Langmuir* **2011**, *27*, 25–29. [CrossRef] [PubMed]
70. Sojoudi, H.; Wang, M.; Boscher, N.D.; McKinley, G.H.; Gleason, K.K. Durable and Scalable Icephobic Surfaces: Similarities and Distinctions from Superhydrophobic Surfaces. *Soft Matter* **2016**, *12*, 1938–1963. [CrossRef] [PubMed]
71. Hu, H.; Gao, L.; Liu, Y. Hydro-/Ice-Phobic Coatings and Materials for Wind Turbine Icing Mitigation. In *Wind Turbine Icing Physics and Anti-/De-icing Technology*; Elsevier: Amsterdam, The Netherlands, 2022; pp. 135–168.
72. Moghtadernejad, S.; Jadidi, M.; Johnson, Z.; Stolpe, T.; Hanson, J. Droplet Impact Dynamics on an Aluminum Spinning Disk. *Phys. Fluids* **2021**, *33*. [CrossRef]
73. Buksh, S.; Almohammadi, H.; Marengo, M.; Amirfazli, A. Spreading of Low-Viscous Liquids on a Stationary and a Moving Surface. *Exp. Fluids* **2019**, *60*. [CrossRef]
74. Hu, H.; Tian, L.; Eluchie, C.; Sista, H.; Hu, H. Comparative Study of Using Superhydrophobic and Icephobic Surface Coatings for Aircraft Icing Mitigation. *AIAA J.* **2024**, *62*, 1588–1600. [CrossRef]
75. Blamey-Beccaria, C.E.A.; Parkes, M.A.; Li, J.; Salzmann, C.G. Ice Nucleation of Aluminum Surfaces. *J. Phys. Chem. C* **2025**, *129*, 11183–11191. [CrossRef]
76. Yin, L.; Xia, Q.; Xue, J.; Yang, S.; Wang, Q.; Chen, Q. In Situ Investigation of Ice Formation on Surfaces with Representative Wettability. *Appl. Surf. Sci.* **2010**, *256*, 6764–6769. [CrossRef]
77. Schutzius, T.M.; Jung, S.; Maitra, T.; Eberle, P.; Antonini, C.; Stamatopoulos, C.; Poulikakos, D. Physics of Icing and Rational Design of Surfaces with Extraordinary Icephobicity. *Langmuir* **2015**, *31*, 4807–4821. [CrossRef] [PubMed]
78. Rioboo, R.; Marengo, M.; Tropea, C. Time Evolution of Liquid Drop Impact onto Solid, Dry Surfaces. *Exp. Fluids* **2002**, *33*, 112–124. [CrossRef]
79. Jin, Z.; Sui, D.; Yang, Z. The Impact, Freezing, and Melting Processes of a Water Droplet on an Inclined Cold Surface. *Int. J. Heat Mass Transf.* **2015**, *90*, 439–453. [CrossRef]
80. Roux, D.C.D.; Cooper-White, J.J. Dynamics of Water Spreading on a Glass Surface. *J. Colloid Interface Sci.* **2004**, *277*, 424–436. [CrossRef] [PubMed]
81. Sikalo, S.; Marengo, M.; Tropea, C.; Ganic, E.N. Analysis of Impact of Droplets on Horizontal Surfaces. In *Proceedings of the Thermal Sciences 2000*; Proceedings of the International Thermal Science Seminar; Begel House Inc.: Danbury, CT, USA, 2000; Volume 1.
82. Liang, G.; Guo, Y.; Yang, Y.; Zhen, N.; Shen, S. Spreading and Splashing during a Single Drop Impact on an Inclined Wetted Surface. *Acta Mech.* **2013**, *224*, 2993–3004. [CrossRef]
83. Tourkine, P.; Le Merrer, M.; Quéré, D. Delayed Freezing on Water Repellent Materials. *Langmuir* **2009**, *25*, 7214–7216. [CrossRef] [PubMed]
84. Beaugendre, H.; Morency, F.; Habashi, W.G. FENSAP-ICE's Three-Dimensional In-Flight Ice Accretion Module: ICE3D. *J. Aircr.* **2003**, *40*, 239–247. [CrossRef] [PubMed]
85. Addy, H.E., Jr.; Miller, D.R.; Ide, R.F. *A Study of Large Droplet Ice Accretion in the NASA Lewis IRT at Near-Freezing Conditions, Part 2*; NASA/TM-107424; NASA Lewis Research Center: Cleveland, OH, USA, 1997.
86. CAV Systems. TKS Ice Protection. Available online: https://www.cav-systems.com/tks/ (accessed on 26 October 2026).
87. Knopf, D.A.; Alpert, P.A. Atmospheric Ice Nucleation. *Nat. Rev. Phys.* **2023**, *5*, 203–217. [CrossRef]
88. Karthika, S.; Radhakrishnan, T.K.; Kalaichelvi, P. A Review of Classical and Nonclassical Nucleation Theories. *Cryst. Growth Des.* **2016**, *16*, 6663–6681. [CrossRef]
89. Maeda, N. Brief Overview of Ice Nucleation. *Molecules* **2021**, *26*, 392. [CrossRef] [PubMed]
90. Kashchiev, D. *Nucleation*; Elsevier: Amsterdam, The Netherlands, 2000.
91. Vali, G.; DeMott, P.J.; Möhler, O.; Whale, T.F. A Proposal for Ice Nucleation Terminology. *Atmos. Chem. Phys.* **2015**, *15*, 10263–10270. [CrossRef]
92. Attinger, D.; Frankiewicz, C.; Betz, A.R.; Schutzius, T.M.; Ganguly, R.; Das, A.; Kim, C.-J.; Megaridis, C.M. Surface Engineering for Phase Change Heat Transfer: A Review. *MRS Energy Sustain.* **2014**, *1*, E4. [CrossRef]
93. Rosky, E.; Cantrell, W.; Li, T.; Nakamura, I.; Shaw, R.A. Molecular Simulations Reveal That Heterogeneous Ice Nucleation Occurs at Higher Temperatures in Water under Capillary Tension. *Atmos. Chem. Phys.* **2023**, *23*, 10625–10642. [CrossRef]
94. Sosso, G.C.; Chen, J.; Cox, S.J.; Fitzner, M.; Pedevilla, P.; Zen, A.; Michaelides, A. Crystal Nucleation in Liquids: Open Questions and Future Challenges in Molecular Dynamics Simulations. *Chem. Rev.* **2016**, *116*, 7078–7116. [CrossRef] [PubMed]
95. Messinger, B.L. Equilibrium Temperature of an Unheated Icing Surface as a Function of Air Speed. *J. Aeronaut. Sci.* **1953**, *20*, 29–42. [CrossRef]
96. Wright, W.B. *User's Manual for LEWICE Version 3.2*; NASA/CR-2008-214255; NASA Glenn Research Center: Cleveland, OH, USA, 2008.
97. Jeck, R.K. *A History and Interpretation of Aircraft Icing Intensity Definitions and FAA Rules for Operating in Icing Conditions*; DOT/FAA/AR-01/91; Federal Aviation Administration: Washington, DC, USA, 2001.

98. Addy, H.E., Jr.; Veres, J.P. *An Overview of NASA Engine Ice-Crystal Icing Research*; NASA/TM-2011-217254; NASA Glenn Research Center: Cleveland, OH, USA, 2011.
99. National Weather Service. Icing Hazards. Available online: https://www.weather.gov/source/zhu/ZHU_Training_Page/icing_stuff/icing/icing.htm (accessed on 25 November 2023).
100. Ferrari, M.; Cirisano, F. Superhydrophobic Coating Solutions for Deicing Control in Aircraft. *Appl. Sci.* **2023**, *13*, 11684. [CrossRef]
101. Federal Aviation Administration. *Turbine Engine and Airframe Sensor Icing Compliance*; Federal Aviation Administration: Washington, DC, USA, 2025.
102. Hu, H.; Al-Masri, F.; Tian, L.; Hu, H. Experimental Study of Dynamic Icing Process on a Pitot Probe Model. *J. Thermophys. Heat Trans.* **2023**, *37*, 632–643. [CrossRef]
103. European Space Agency ESA. Operations Begin to De-Ice Euclid's Vision. Available online: https://www.esa.int/Science_Exploration/Space_Science/Euclid/Operations_begin_to_de-ice_Euclid_s_vision (accessed on 24 March 2024).
104. Malik, Y.A.; Karpen, N.; Bonaccurso, E.; Roisman, I.; Hussong, J.; Villedieu, P. Experimental Investigation of the Accretion and Shedding Process on a Heatable NACA0012 Airfoil in Ice Crystal Icing Conditions. *Cold Reg. Sci. Technol.* **2024**, *217*, 104030. [CrossRef]
105. Lin, Y.; Chen, H.; Wang, G.; Liu, A. Recent Progress in Preparation and Anti-Icing Applications of Superhydrophobic Coatings. *Coatings* **2018**, *8*, 208. [CrossRef]
106. Xu, X.; Zhang, Y.; Zhang, Y.; Wang, H.; Wang, T.; Chen, G. Uncertainty Qualification of Aerodynamic Performance of a Swept Wing with Ice Accretion. *Chin. J. Aeronaut.* **2025**, *38*, 103332. [CrossRef]
107. von Hardenberg, P. Introduction to Aircraft Icing and NASA's Approach to Understanding It. In Proceedings of the ASME Baltimore Section Lecture Series, Baltimore, MD, USA, 6 April 2022; NASA Document ID 20220005049.
108. Yamazaki, M.; Jemcov, A.; Sakaue, H. A Review on the Current Status of Icing Physics and Mitigation in Aviation. *Aerospace* **2021**, *8*, 188. [CrossRef]
109. Han, N.; Siddique, M.A.; Zhang, Z.; Tian, L.; Hu, H.; Hu, H. A Flight-Testing Campaign to Examine Inflight Icing Characteristics and Its Effects on the Flight Performance of an Unmanned-Aerial-Vehicle. *Cold Reg. Sci. Technol.* **2023**, *207*, 103775. [CrossRef]
110. Tian, L.; Hu, H.; Veerakumar, R.; Hu, H. Ice Accretion Characteristics on Rotating Aeroengine Fan Blades. *Exp. Therm. Fluid Sci.* **2024**, *155*, 111181. [CrossRef]
111. National Transportation Safety Board (NTSB). U.S. Civil Aviation Accident Dashboard: 2008–2024. Available online: https://www.ntsb.gov/safety/StatisticalReviews/Pages/CivilAviationDashboard.aspx (accessed on 8 August 2026).
112. CAST/ICAO Common Taxonomy Team (CICTT). Aviation Occurrence Categories: Definitions and Usage Notes; Version 4.8, May 2021. Available online: https://www.enac.gov.it/app/uploads/2024/04/CICTT_Occurrence_Category_4.8_May_2021.pdf (accessed on 9 November 2026).
113. National Transportation Safety Board (NTSB). *Engine Power Loss Due to Carburetor Icing: Recognizing Weather Conditions and Applying Simple Procedures Can Prevent Avoidable Accidents*; Safety Alert SA-029; NTSB: Washington, DC, USA, 2015.
114. Eick, D. Aircraft Icing Accidents. In Proceedings of the In-Flight Icing Users Technical Interchange Meeting (TIM), Washington, DC, USA, 25–26 February 2015.
115. Federal Aviation Administration. In-Flight Icing. Available online: https://www.faa.gov/nextgen/programs/weather/awrp/ifi (accessed on 10 December 2023).
116. Bureau d'Enquêtes et d'Analyses pour la Sécurité de l'Aviation Civile (BEA). *Final Report on the Accident on 1 June 2009 to the Airbus A330-203 Registered F-GZCP Operated by Air France, Flight AF 447 Rio de Janeiro–Paris*; BEA: Le Bourget, France, 2012. Available online: https://bea.aero/en/investigation-reports/notified-events/detail/accident-to-the-airbus-a330-203-registered-f-gzcp-and-operated-by-air-france-occured-on-06-01-2009-in-the-atlantic-ocean/ (accessed on 26 October 2026).
117. Wang, Z. Recent Progress on Ultrasonic De-Icing Technique Used for Wind Power Generation, High-Voltage Transmission Line and Aircraft. *Energy Build.* **2017**, *140*, 42–49. [CrossRef]
118. Pourbagian, M.; Habashi, W. Aero-Thermal Optimization of In-Flight Electro-Thermal Ice Protection Systems in Transient de-Icing Mode. *Int. J. Heat Fluid Flow* **2015**, *54*, 167–182. [CrossRef]
119. Tian, Z.; Wang, L.; Zhu, D.; Chen, C.; Zhao, H.; Peng, R.; Zhang, H.; Fan, P.; Zhong, M. Passive Anti-Icing Performances of the Same Superhydrophobic Surfaces under Static Freezing, Dynamic Supercooled-Droplet Impinging, and Icing Wind Tunnel Tests. *ACS Appl. Mater. Interfaces* **2023**, *15*, 6013–6024. [CrossRef] [PubMed]
120. Kim, Y.; Yee, K. Target Temperature-Based Simulation Method for Predicting Performance and Designing Aircraft Thermal Anti-Icing Systems. *Int. J. Heat Mass Transf.* **2024**, *229*, 125688. [CrossRef]
121. Chu, Z.; Geng, J.; Yang, Q.; Yi, X.; Dong, W. Prediction of Temperature Distribution on an Aircraft Hot-Air Anti-Icing Surface by ROM and Neural Networks. *Aerospace* **2024**, *11*, 930. [CrossRef]
122. Jiang, X.; Wang, Y. Studies on the Electro-Impulse De-Icing System of Aircraft. *Aerospace* **2019**, *6*, 67. [CrossRef]
123. Wang, Y.; Xu, Y.; Huang, Q. Progress on Ultrasonic Guided Waves De-Icing Techniques in Improving Aviation Energy Efficiency. *Renew. Sustain. Energy Rev.* **2017**, *79*, 638–645. [CrossRef]

124. Palanque, V.; Planes, T.; Pommier-Budinger, V.; Budinger, M.; Delbecq, S. Piezoelectric Resonant Ice Protection Systems—Part 2/2: Benefits at Aircraft Level. *Chin. J. Aeronaut.* **2024**, *37*, 50–63. [CrossRef]
125. Piscitelli, F.; Chiariello, A.; Dabkowski, D.; Corraro, G.; Marra, F.; Di Palma, L. Superhydrophobic Coatings as Anti-Icing Systems for Small Aircraft. *Aerospace* **2020**, *7*, 2. [CrossRef]
126. Korga, S. Real-Time Image Analysis for Intelligent Aircraft De-Icing Decision Support Systems. *Appl. Sci.* **2025**, *15*, 7752. [CrossRef]
127. Yan, Y.; Tang, C.; Huang, J.; Cen, Z.; Xie, Z. Visual Detection on Aircraft Wing Icing Process Using a Lightweight Deep Learning Model. *Aerospace* **2025**, *12*, 627. [CrossRef]
128. Farina, D.; Machrafi, H.; Queeckers, P.; Dongo, P.D.; Iorio, C.S. Innovative AI-Enhanced Ice Detection System Using Graphene-Based Sensors for Enhanced Aviation Safety and Efficiency. *Nanomaterials* **2024**, *14*, 1135. [CrossRef] [PubMed]
129. Abdelghany, E.S.; Farghaly, M.B.; Almalki, M.M.; Sarhan, H.H.; Essa, M.E.-S.M. Machine Learning and IoT Trends for Intelligent Prediction of Aircraft Wing Anti-Icing System Temperature. *Aerospace* **2023**, *10*, 676. [CrossRef]
130. Li, S.; Qin, J.; He, M.; Paoli, R. Fast Evaluation of Aircraft Icing Severity Using Machine Learning Based on XGBoost. *Aerospace* **2020**, *7*, 36. [CrossRef]
131. European Union Aviation Safety Agency (EASA). Artificial Intelligence and Aviation. Available online: https://www.easa.europa.eu/en/light/topics/artificial-intelligence-and-aviation-0 (accessed on 24 August 2026).
132. Mousavi, S.M.; Sotoudeh, F.; Chun, B.; Lee, B.J.; Karimi, N.; Faroughi, S.A. The Potential for Anti-Icing Wing and Aircraft Applications of Mixed-Wettability Surfaces—A Comprehensive Review. *Cold Reg. Sci. Technol.* **2024**, *217*, 104042. [CrossRef]
133. Feng, L.; Li, S.; Li, Y.; Li, H.; Zhang, L.; Zhai, J.; Song, Y.; Liu, B.; Jiang, L.; Zhu, D. Super-Hydrophobic Surfaces: From Natural to Artificial. *Adv. Mater.* **2002**, *14*, 1857–1860. [CrossRef]
134. Ensikat, H.J.; Ditsche-Kuru, P.; Neinhuis, C.; Barthlott, W. Superhydrophobicity in Perfection: The Outstanding Properties of the Lotus Leaf. *Beilstein J. Nanotechnol.* **2011**, *2*, 152–161. [CrossRef] [PubMed]
135. Zhang, Y.; Meng, N.; Babar, A.A.; Wang, X.; Yu, J.; Ding, B. Multi-Bioinspired and Multistructural Integrated Patterned Nanofibrous Surface for Spontaneous and Efficient Fog Collection. *Nano Lett.* **2021**, *21*, 7806–7814. [CrossRef] [PubMed]
136. Jiang, X.; Zhuo, Y.; Wang, P.; Yang, M.; Liao, Y.; Chen, B. The Perspectives of Hydrophobic Coatings for Mitigating Icing on Atmospheric Structures. *Coatings* **2023**, *13*, 326. [CrossRef]
137. Tian, Y.; Wang, Q.; Liu, M.; Zhang, J.; Zhou, L. Robust and Quantitative Characterization of Aircraft Icing with Mode and Frequency Selective Ultrasonic Guided Wave. *Ultrasonics* **2023**, *127*, 106846. [CrossRef] [PubMed]
138. Wang, Y.; Wang, Y.; Chen, S.; Zhu, C.; Wu, D.; Zhu, C.; Lu, X. Focused Ultrasonic Transducer for Aircraft Icing Detection. *Ultrasonics* **2025**, *147*, 107509. [CrossRef] [PubMed]
139. Wang, Y.; Zhang, Y.; Wang, Y.; Zhu, C.; Zhao, N.; Zhu, C. Early Warning and Thickness Measurement of Aircraft Icing Using Ultrasonic Pulse Echoes. *Proc. Inst. Mech. Eng. G J. Aerosp. Eng.* **2025**, *239*, 847–863. [CrossRef]
140. Electronic Code of Federal Regulations (eCFR). Title 14, Part 25—Airworthiness Standards: Transport Category Airplanes. Appendix C (Icing Conditions) and Appendix O (Supercooled Large Drop Icing Conditions). Available online: https://www.ecfr.gov/current/title-14/chapter-I/subchapter-C/part-25 (accessed on 1 October 2026).

Disclaimer/Publisher's Note: The statements, opinions and data contained in all publications are solely those of the individual author(s) and contributor(s) and not of MDPI and/or the editor(s). MDPI and/or the editor(s) disclaim responsibility for any injury to people or property resulting from any ideas, methods, instructions or products referred to in the content.